Fall 2012

A hybrid brain-computer interface based on motor intention and visual working memory

Ching-Chang Kuo
Louisiana Tech University

A HYBRID BRAIN-COMPUTER INTERFACE

BASED ON MOTOR INTENTION AND

VISUAL WORKING MEMORY

by

Ching-Chang Kuo, B.Eng., M.S.

A Dissertation Presented in Partial Fulfillment
of the Requirements of the Degree
Doctor of Philosophy

COLLEGE OF ENGINEERING AND SCIENCE
LOUISIANA TECH UNIVERSITY

November 2012

UMI Number: 3534297

UMI 3534297

LOUISIANA TECH UNIVERSITY

THE GRADUATE SCHOOL

<u>JULY 16, 2012</u>
Date

We hereby recommend that the dissertation prepared under our supervision by

Ching-Chang Kuo, B.Eng., M.S.

entitled **A Hybrid Brain-Computer Interface based on Motor Intention and**

Visual Working Memory

be accepted in partial fulfillment of the requirements for the Degree of

Doctor of Philosophy in Biomedical Engineering
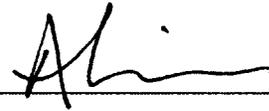
Supervisor of Dissertation Research

Head of Department

Department

Recommendation concurred in:
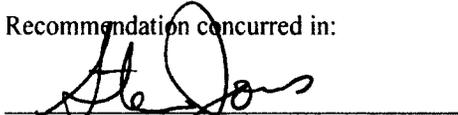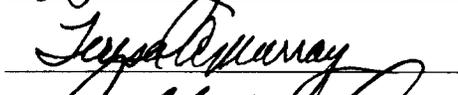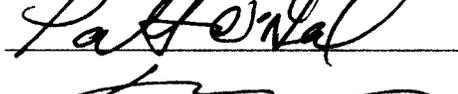
Advisory Committee

Approved:

Director of Graduate Studies

Dean of the College

Approved:

Dean of the Graduate School
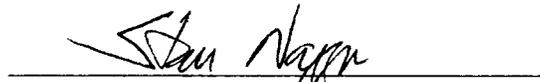
ABSTRACT

Non-invasive electroencephalography (EEG) based brain-computer interface (BCI) is able to provide alternative means for people with disabilities to communicate with and control over external assistive devices. A hybrid BCI is designed and developed for following two types of system (control and monitor).

Our first goal is to create a signal decoding strategy that allows people with limited motor control to have more command over potential prosthetic devices. Eight healthy subjects were recruited to perform visual cues directed reaching tasks. Eye and motion artifacts were identified and removed to ensure that the subjects' visual fixation to the target locations would have little or no impact on the final result. We applied a Fisher Linear Discriminate (FLD) analysis for single-trial classification of the EEG to decode the intended arm movement in the left, right, and forward directions (before the onsets of actual movements). The mean EEG signal amplitude near the PPC region 271-310 ms after visual stimulation was found to be the dominant feature for best classification results. A signal scaling factor developed was found to improve the classification accuracy from 60.11% to 93.91% in the two-class (left versus right) scenario. This result demonstrated great promises for BCI neuroprosthetics applications, as motor intention decoding can be served as a prelude to the classification of imagined motor movement to assist in motor disable rehabilitation, such as prosthetic limb or wheelchair control.

The second goal is to develop the adaptive training for patients with low visual working memory (VWM) capacity to improve cognitive abilities and healthy individuals who seek to enhance their intellectual performance. VWM plays a critical role in preserving and processing information. It is associated with attention, perception and reasoning, and its capacity can be used as a predictor of cognitive abilities. Recent evidence has suggested that with training, one can enhance the VWM capacity and attention over time. Not only can these studies reveal the characteristics of VWM load and the influences of training, they may also provide effective rehabilitative means for patients with low VWM capacity. However, few studies have investigated VWM over a long period of time, beyond 5-weeks.

In this study, a combined behavioral approach and EEG was used to investigate VWM load, gain, and transfer. The results reveal that VWM capacity is directly correlated to the reaction time and contralateral delay amplitude (CDA). The approximate "magic number 4" was observed through the event-related potentials (ERPs) waveforms, where the average capacity is 2.8-item from 15 participants. In addition, the findings indicate that VWM capacity can be improved through adaptive training. Furthermore, after training exercises, participants from the training group are able to improve their performance accuracies dramatically compared to the control group. Adaptive training gains on non-trained tasks can also be observed at 12 weeks after training".

Therefore, we conclude that all participants can benefit from training gains, and augmented VWM capacity can be sustained over a long period of time. Our results suggest that this form of training can significantly improve cognitive function and may be useful for enhancing the user performance on neuroprosthetics device.

APPROVAL FOR SCHOLARLY DISSEMINATION

The author grants to the Prescott Memorial Library of Louisiana Tech University the right to reproduce, by appropriate methods, upon request, any or all portions of this Dissertation. It is understood that "proper request" consists of the agreement, on the part of the requesting party, that said reproduction is for his personal use and that subsequent reproduction will not occur without written approval of the author of this Dissertation. Further, any portions of the Dissertation used in books, papers, and other works must be appropriately referenced to this Dissertation.

Finally, the author of this Dissertation reserves the right to publish freely, in the literature, at any time, any or all portions of this Dissertation.

Author _Ching - Chang Ko_

Date _09 / 24 / 12_

TABLE OF CONTENTS

LIST OF FIGURES

LIST OF TABLES

ACKNOWLEDGMENTS

I am deeply grateful to my advisor Dr. Alan Chiu whose guidance and encouragement inspired me in all the time of research for and writing this dissertation.

I also want to thank my committee members for their support. They advised me on how to write my proposal.

Thanks Dr. June Feng and Cheng Zhang for our collaboration project.

Thanks Dr. Tersea A. Murray for helpful comments and suggestions to my manuscript.

Thanks volunteers for participating in my research and to lab members for their comments and suggestions.

Lastly, I thank the College of Engineering and Science at Louisiana Tech University and National Institutes of Health (NIH) National Center for Research Resources (NCRR) for funding and support.

CHAPTER 1

INTRODUCTION

1.1   BCI Control System

Brain Computer Interface (BCI) is a frontier research area in neural engineering that has gathered a great deal of attention from scientists and the general public. BCI technology allows communication to occur between the brain and an external machine [1], and its application can range from entertainment to assistive devices [2]. In a typical BCI system, the brain activities are recorded and processed by a computer system, which in turn, deciphers the mental or physical activities and creates commands to control external devices [3, 4]. A brain-computer interface device is shown in Figure 1.
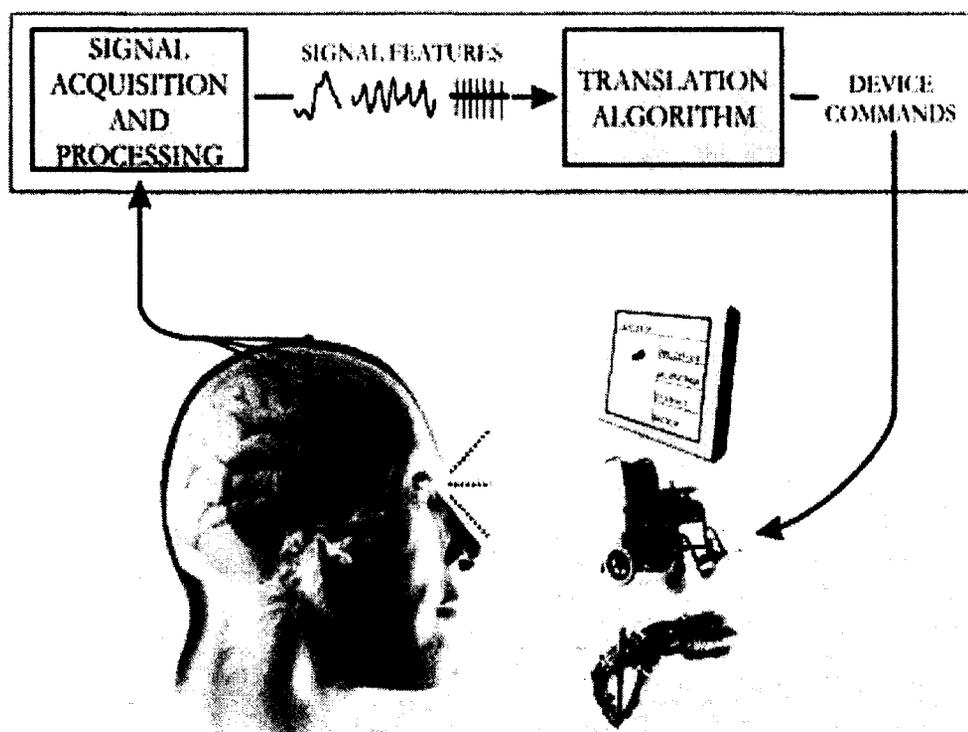
Figure 1: A brain-computer interface device [5].

One of the goals in BCI and neural engineering research is creating assistive devices for those with limited motor control. A successful BCI system is valuable in motor disable rehabilitation by allowing the subjects to perform physical practices [6]. This type of technology would drastically improve the quality of life for the patients by allowing these individuals to have better communication and more independent control over the assistive devices [7, 8].

The operation of traditional electromyogram (EMG)-based controlled prosthetics is based on the decoding of myoelectric signals of residual muscles [9, 10]. While these devices provide more basic control over the prostheses, certain limitations restrict their acceptability. Users with severely limited motor ability would require much effort to learn how to contract specific muscle groups in order to control the device. The number of these distinctive muscle contractions is related to the degrees of freedom (DoF) of the

device. The movements of these muscle contractions are often unnatural and may interfere with the individual's social interactions. Therefore, the need to create a more intuitive control strategy based on the user's naturally occurring brain signals is apparent. Figure 2 shows the difference between classical (EMG based) control and the new (brain wave) control of prosthesis.
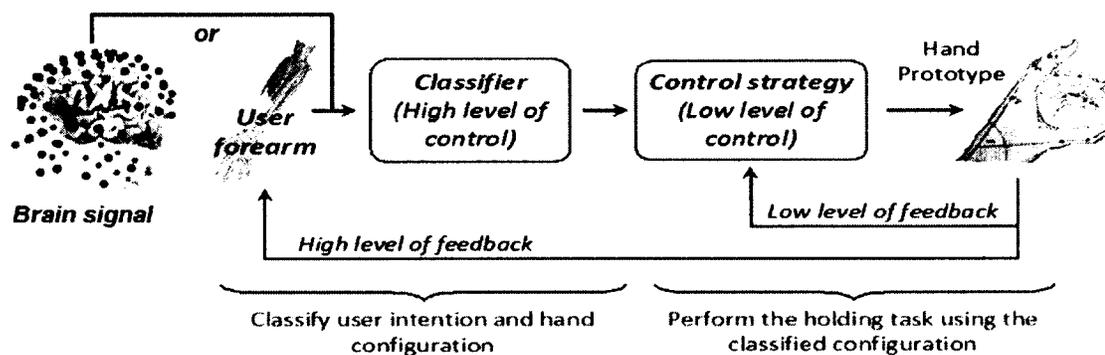
Figure 2: The classical (EMG based) and the new (brain wave) control of prosthesis.

The use of BCI can eliminate the user's need to learn different muscle contractions, then reducing the amount of cognitive interaction required for rehabilitation applications. The BCI technology today encompasses invasive electrocorticography (ECoG), implanted electrodes, or non-invasive electroencephalography (EEG) [11]. Current literature suggests that EEG is adequate to extract detailed information about precise movements of the upper limb [12]. Non-invasive techniques based on EEG surface potentials appear to be a more sensible method for collecting and processing data [13-15] for neuroprosthetics applications with relatively few DoFs (such as prosthetic arm control). With the use of surface EEGs, the user's intentional movements can be decoded. Real-time signal classification based on the activation and feature extraction from particular brain regions can allow for the control of the assistive devices.

When examining the neuronal activities for BCI applications, the signal intensity or signal power features has been commonly used for decoding user movement intents. The posterior parietal cortex (PPC) region is responsible for converting visual stimuli into motor movements [16] and is a vital location for decoding intended motor movement [13]. While most other research focused on discriminating EEG signals between left hand, right hand, toe, and tongue imagined movement [17, 18], our endeavor is to decode and classify EEG signals for the intended movement direction of the same limb, leading to a more realistic control of a single upper limb prosthetic arm [19]. Single-trial signal classification strategy was developed to evaluate the temporal, spatial, and spectral EEG features during the planning stages of motor movements in the left, right, and forward directions similar to [20-22]. Ultimately, such classification algorithm will be a part of a two-stage neuroprosthetics control strategy. In the first stage, the intended motor movement directions can be decoded using EEG signal features. The second stage is envisioned to be a motor imaginary classifier. In this paper, we shall focus our discussion on the classification of motor intention only.

Since the presentation of different types of visual cues does not influence the performance [23], we used "realistic" instead of "abstract" visual-cue in order to avoid a tedious calibration procedure. Furthermore, realistic visual image environment may enhance the learning progress in a BCI task [24]. Ensemble Empirical Mode Decomposition (EEMD), where the signals are decomposed into intrinsic mode functions (IMF) [25], was utilized to isolate the frequency information in the training set.

We developed and validated the use of scalp EEG data and current density localization for intended movement direction analysis. Subsequently, we evaluate the

feature classification strategy suitable for distinguishing the brain activity associated with the intended hand movement. Potential variations in electrode impedance at different recording locations and at different recording times may drastically impact the amplitude and signal-to-noise ratio (SNR) of the EEG signals. This would considerably hinder the performance of any amplitude-based signal classifiers. Finally, we proposed and evaluated a scaling factor based on the "signature" EEG signal after the presentation of the visual-cues. We hypothesize that such scaling factor is able to compensate the potential problems of electrode impedance differences between trials and across different locations. Our preliminary result indicated that the inclusion of such a scaling process would significantly improve the overall single-trial signal classification accuracy. In a two-class decoding scheme, the accuracy improved from approximately 60% to over 90% with the scaling factor. The implication of this work would have direct impact on the acceptability of the BCI neuroprosthetics application as the new device will function based on user's intent, which can provide a more intuitive control paradigm, for simple device control with few DoFs.

1.2   BCI Monitor System

Visual working memory (VWM) , or visual short-term memory, refers to a limited amount of information storage within a few seconds [26]. It is associated with important cognitive modalities, including attention, perception, reasoning, comprehension, and language acquisition [27, 28]. VWM also plays a critical role in preserving and processing information, and its capacity can be used as a predictor of cognitive abilities [29]. For instance, researchers have focused on VWM capacity changes to identify healthy or memory-impaired individuals suffering from attention-

deficit hyperactivity disorder (ADHD), schizophrenia, stroke [30], or memory deficiencies related to aging [31, 32]. Recent evidence has suggested that brain training can enhance an individual's VWM capacity and attention over time [31] by increasing the activity in the prefrontal cortex, the parietal cortex, and the basal ganglia [33]. Not only can these studies reveal the characteristics of VWM load and the influences of training, they may also provide effective rehabilitative means for patients with low VWM capacity. Furthermore, healthy individuals who seek to enhance their intellectual performance may also benefit from the adaptive training [33]. This method could also be used with brain computer interfaces to repair or augment human cognitive function [34].

Despite the potential applications of VWM, very few studies have investigated VWM over a long period of time, beyond 5-weeks. Most of the research has been concentrated on distinguishing different memory systems and memory-processing phases to build up a category of memory systems and their functions [35]. Considering the importance of VWM, a combined behavioral and electrophysiological approach was used to reveal the impact of VWM load, training, and transfer effects on individuals' memory capacities and task-related performances. The event-related potentials (ERPs) as the result of VWM information processing were recorded. Arrays of colored squares were used to estimate the VWM capacity through computerized tasks, broken into several experimental blocks.

The goal of this study was to evaluate training paradigms to expand memory capacity and improve VWM performance. We hypothesized that participants would dramatically improve their neural activities in raising attention and memorization. Overall, three major experiments were conducted. (1) VWM load experiments. We

estimated the VWM capacity behaviorally through accuracy measurements, and electrophysiologically through the level of CDA. (2) VWM training gains experiment. VWM adaptive training was developed to expand memory capacity and general cognitive improvement over a period of 12-weeks. (3) VWM transfer benefits experiment. Subjects were separated into two groups, training and control groups, to evaluate the behavior evidence and neural activity. The transfer benefits were calculated by comparing between pre-training and post-training. We conclude that VWM can be improved by adaptive training across time, that all subjects benefit from training tasks, and that they show sustained improvement on VWM capacity over a long period of time.

CHAPTER 2

BACKGROUND

2.1   Brain-Computer Interface

Brain-Computer Interface (BCI) or Brain-Machine Interface (BMI) has caught much attention in the past few years not only by scientists and engineering forces in understanding brain function and by impressive application but also people have a brief idea from the movie *Avatar*. The signals used for BCI can be collected either invasively or non-invasively. The invasive approach uses electrodes implanted on the surface of the cortex, known as Electrocorticography (ECoG). The non-invasive approach uses Electroencephalography (EEG), in which electrodes are placed on the scalp. There are some various steps in the non-invasive based BCI cycle as shown in Figure 3, such as measurement of brain activities, single preprocessing, feature extraction, pattern recognitions classification and device commands. We believe BCI research should translate into practical applications for the healthy and disabled users as well as into novel ways of analysis neurophysiology data because these developments will have significant impact on our lives [11]. Figure 4 shows the current Prototype device designed in our neural signals and systems laboratory [19].
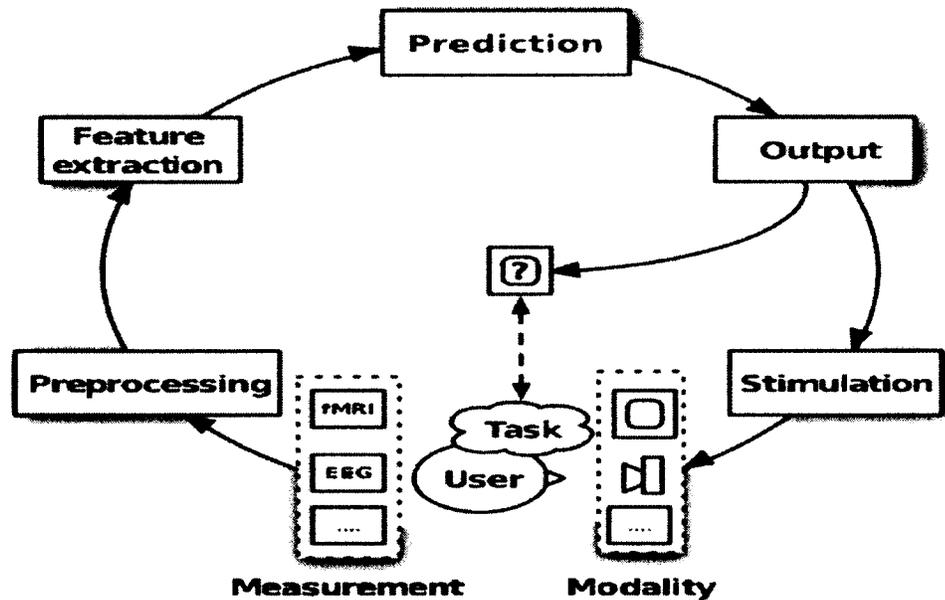
Figure 3: A typical BCI [11].
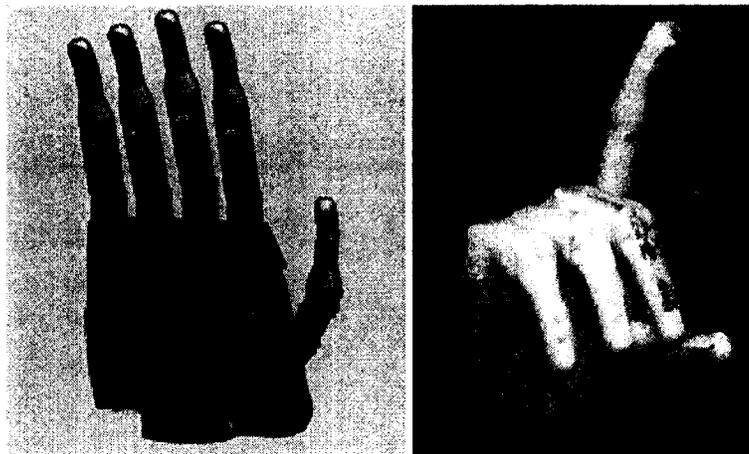
Figure 4: (Left) The CAD model of the low-cost robotic hand is illustrated using SolidWorks software. (Right) Prototype of the robotic hand is covered with a silicone glove, which helps to protect the components and to faciliate a secure grip [19].

2.2   Electroencephalographic (EEG)

2.2.1   Introduction of EEG

EEG is an important tool for studying neural activity in a human. It uses a non-invasive brain imaging method by recording electric potential differences on the scalp

[36]. The electrical charges are maintained by billions of neurons. Neurons constantly exchange ions with an extracellular medium. The volume conduction process is defined as many ions pushed out of many neurons at the same time to generate a wave. The wave reaches the surface and picks up by the electrodes [37].

EEG is measured by these electrodes and recorded as voltages over time. Localizing the different modules of the functional network in a given mental task is the principal aim of functional neuroimaging studies [38]. To investigate whether EEG signals recorded from a human can be used to decode intended movement direction, we recorded the whole head EEG with eye movement and reach task and find the direction related modulation of event-related potentials (ERPs).

Neural activity associated with different movement directions can be distinguished using EEG recording and might be used to drive the brain-computer interface applications [13]. It has been assumed that these parameters can be derived accurately only from a signal recorded by electrodes, but the long-term stability of the brain-computer interface is the electrodes are not uncertain by the conductivity value [39].

2.2.2   Wave Patterns and Brain Functions

Source EEG activity exhibits oscillatory behavior at different frequency ranges and spatial distributions for different brain functions. Most of the brain signals observed from the surface EEG falls in the range of 0.1~30 Hz due to the EEG technique limitation. Below or above this range is often seen as artifacts [40]. A typical wave pattern in EEG is shown in Figure 5. The Delta band is the slowest with the highest

amplitude ranges up to 4 Hz. Theta is between 4 ~ 7 Hz, Alpha is 8 ~ 12 Hz, Beta is 12 ~ 30 Hz, Gamma is 30 ~ 100 Hz, and Mu is 8 ~ 13 Hz.
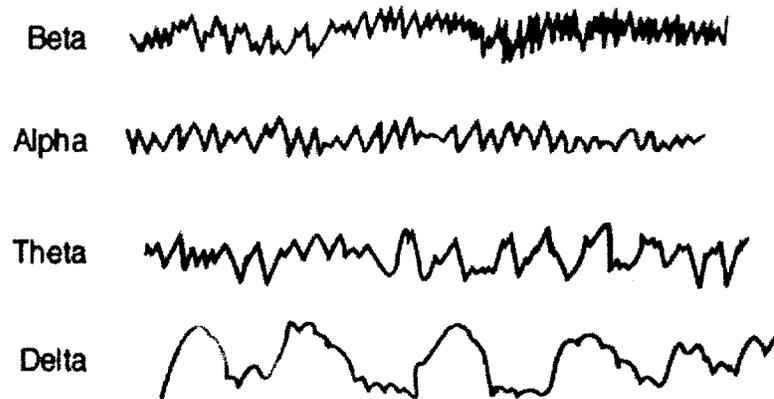
Figure 5: A typical wave patterns in EEG.

The brain provides coherent control over the interplay between different subsystems such as information processing, perception, motor control, arousal, homeostasis, motivation, learning and memory [41]. The cortical input and output pathways are shown in Figure 6. Previous research in the localization of brain function indicates regions that could provide signals that are particularly useful for BCI. In general, motor intention and visual working memory studies involved include the prefrontal cortex, the parietal cortex, the motor cortex, and the basal ganglia [33]. The posterior parietal cortex especially plays an important role in visual intention and VWM that processes the visual information about the structure of the environment. Next, PPC analyzes the information. With memory of past circumstances, it generates motor response comments. Finally, PPC is involved in motor control by producing body movements [42].

PPC Input and Output Pathways

Posterior parietal
association cortex

Areas of secondary
motor cortex

Dorsolateral
prefrontal
association
cortex

Visual
cortex

Somatosensory
cortex

Auditory
cortex
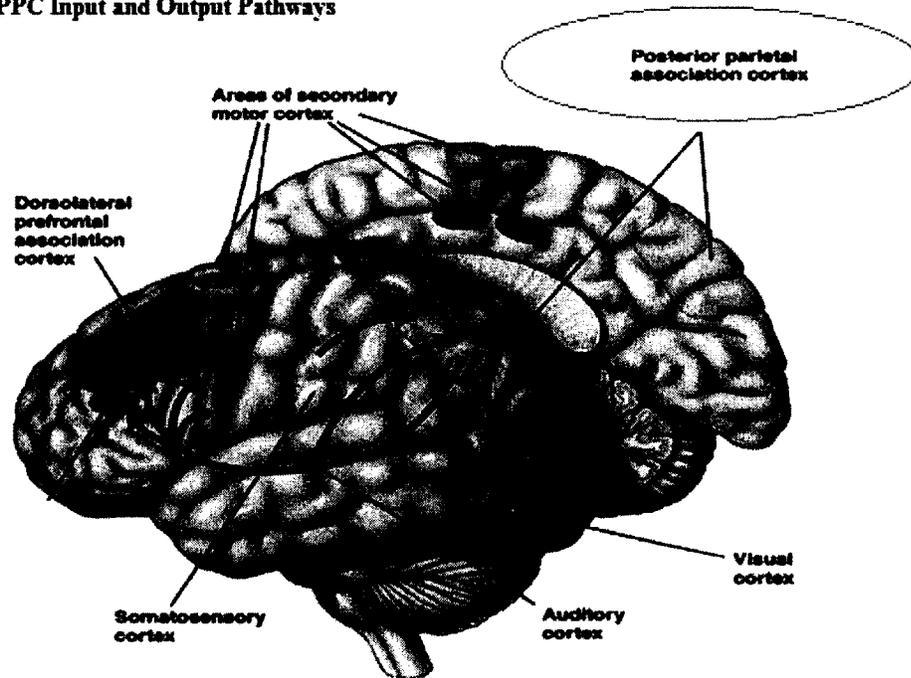
Figure 6: Cortical input and output pathways [43].

2.2.3   Neuroimaging Techniques

When you insert a figure, you may need to adjust its formatting. To view the borders of the table, click on the figure, click on the table, and then click on the "Layout" ribbon. (The "Layout" ribbon will not appear until you click on the figure or other content within the table). The The most important limitation in EEG is poor spatial resolution, but EEG is sensitive and accurate because the device can directly detect the neural activity changes from scalp electrodes [44]. Likewise, compared to other neuroimaging methods [45, 46], such as functional magnetic resonance image (fMRI), EEG is low cost, less time consuming and easier to operate. It is simple to modify our EEG-based visual tasks to other paradigms to study visual intention and VWM. Another important difference between EEG and fMRI is that EEG is able to resolve hemodynamic changes of integrated cognitive activity over milliseconds, while the fMRI only requires

the resolution over a few seconds [47]. As a result, EEG is more suitable for the understanding of short term memory representation, and predict one's cognitive ability through VWM tasks. Currently, various hardware and software advancements have improved both resolution and noise reduction for EEG. One improvement has been the increase from 64 to 128 and 256 electrodes for sensor nets [2]. Additionally, software has been developed that effectively removes the noise, providing a cleaner EEG signal. Although the capacitance of the cell membrane tends to filter the higher gamma frequencies, some studies have found features at these higher frequency bands [39, 48]. Functional near-infrared spectroscopy (fNIRS) is another method which measures changes in blood hemoglobin concentrations linked with neural activities [49]. EEG and fNIRS are much more portable than the fMRI machine allow us to freely move the subjects. However, fNIRS only can scan the cortical cortex compared to the fMRI which measures throughout the whole brain [50]. The invasive method ECoG provides high spatial resolution and better signal fidelity from artifacts such as eye movement [39]. The main obstacle for this approach comes from the development of infections or the creation of scar tissue from the immune system that insulate the electrodes over time. A secondary problem is the difficulty in getting approval for research on human subjects due to the inherent risk to the patients. Moreover, the participants of these studies are generally non-healthy individuals and the results might be limited or affected by their ailments [51]. Figure 7 is shown as the EEG resolution compared to other common measurement methods for BCI.
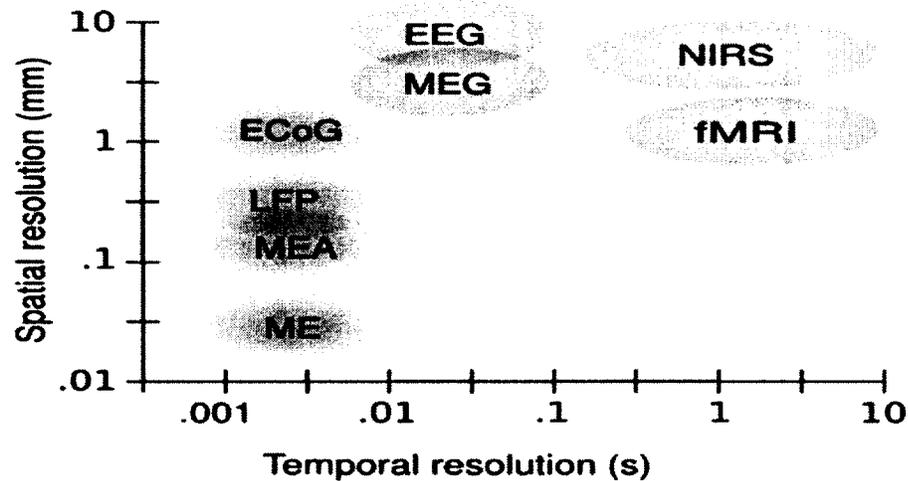
Figure 7: Overview of the scale of spatial and temporal resolution of measurement methods used for BCI. Non-invasive methods are shown in blue and invasive methods are shown in red [11].

2.3   The Estimation of Source Localization

There are some common questions about source localization: 1) where is the source? 2) what are the orientations? and 3) how does source field pass through the subject's head to the recoding electrodes? Forward and inverse modelings are the first problem for EEG/ERP researchers. A biophysical solution to this inverse problem must start with construction of a forward head model for individual users, but it requires extensive computation and expensive MR Head images and needs to develop EEG electrodes into a 3D functional brain image modality. A different purpose might require various degrees of anatomic accuracy. So, using a standard head model may suffice for our research since we do not have a MRI machine. For the inverse problem, we look for a simple map representing the only one activation source, which is easy to classify the source and location. So, utilizing the independent component analysis as an unsupervised spatial filtering technique can extract the EEG's independent component activities without abnormal movement (eye movement, eye blink, and muscle signals) as well as

brain signal from other functional processes [52]. Figure 8 shows the spatiotemporal filter for extracting activity from multiple cortical sources.

$x(t) = As(t)$
Observed
multi-channel EEG

unknown mixing process *BLIND SEPARATION (learnt weights)*

$u(t) = Wx(t)$
Activity from Independent Cortical Sources
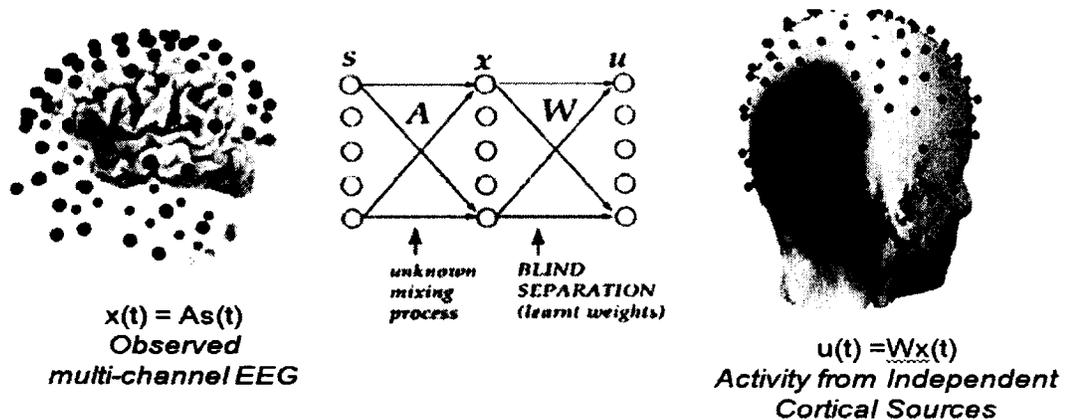
Figure 8: A Spatiotemporal Filter for extracting activity from multiple cortical sources.

DIPFIT stands for equivalent dipole source localization of independent components. DIPFIT 2.0 toolbox is an EEGLAB plug-in based on functions written and contributed by Robert Oostenveld, and docked to EEGLAB [53]. DIPFIT 2.0 includes two types of scalp map. By draft, the spherical four shell model uses four spherical surfaces to model the brain. The boundary element model is comprised of three 3D surface extracted from MNI. In general, the BEM is more realistic than the four spheres model, and will get back more precise results. Nevertheless, BEM is a numerical model whereas the spherical is an analysis model. Sometimes BEM leads to an incorrect solution due to numerical instabilities [53]. Figure 9 shows the BEM model which we are used for this project and the illustration in Figure 10 is of dipoles using BEM mode for independent components (ICs) 1, 3 and 6 from our intended arm reaching movement data.
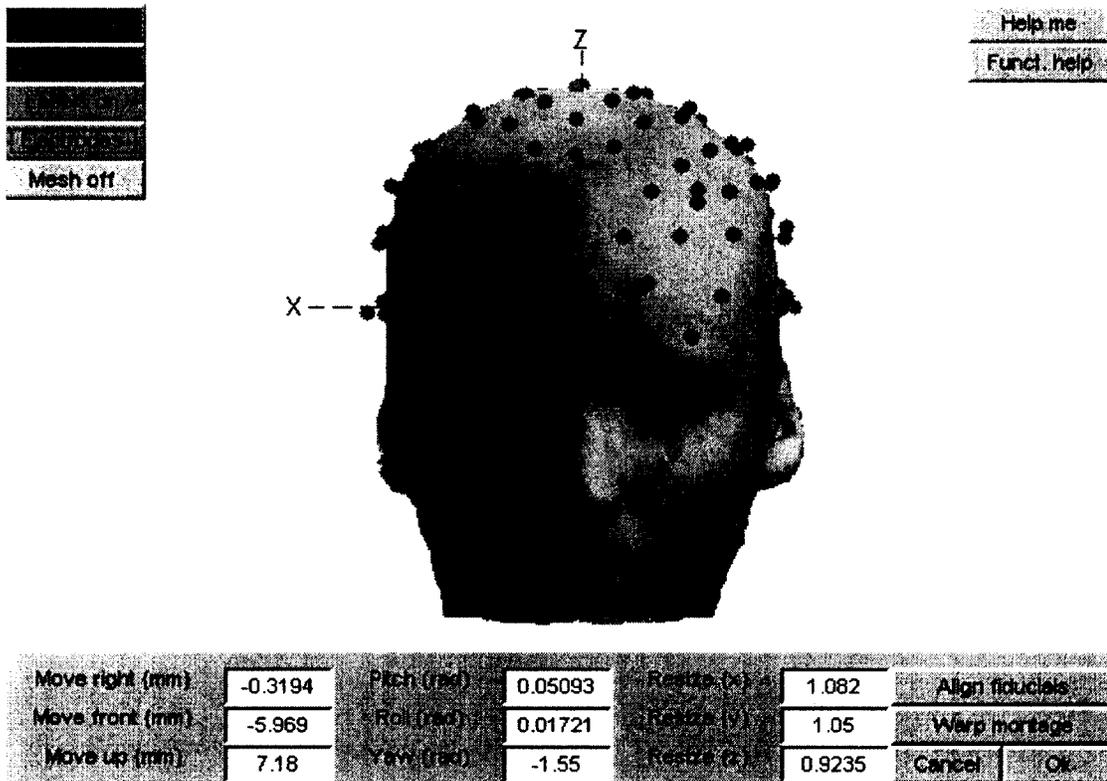
Figure 9: Boundary Element Model coordinate system [53].
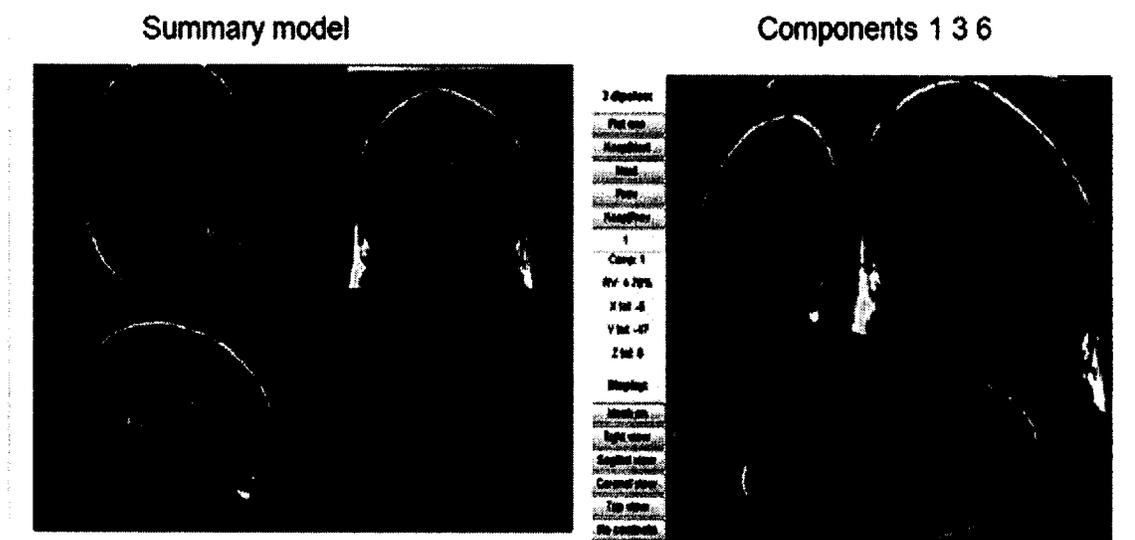
Figure 10: Illustration of dipoles using BEM mode for ICs 1,3 and 6 [53].

2.4   Biological Artifacts

2.4.1   Independent Component Analysis (ICA)

Independent component analysis (ICA) has been widely used in EEG analysis. It can decompose the overlapping source activities constituting the scalp EEG into functionally specific component processes [13]. EEGLAB toolbox v.9 in Matlab was used in the analysis of the intended arm movement [53]. Independent component analysis (ICA) was used to remove artifacts and to reduce the dimensionality of the data. The extended informax ICA method algorithm was used to decompose the signals. Bad trials containing abnormal values and artifacts, such as eye movement, eye blinks, and muscle signals were removed. Figure 11 shows some typical components of abnormal signals of brain. Data constraints for ICA recommend it is optimal to decompose a number of times, more than 20 times the number of the channels squared. In my study, 128 channels data $20*128^2$ time points at 128 points/sec will require over 42 min, about 750 MB data ($20*128^2/(128*60) \cong 42$).

ICA should be zero-mean. Any re-referencing of the data does not change its information content or its source. The impact of the sampling rate is unknown in the field of ICA decomposition. ICA roles to single trials and ERPs by the definition and design independent component processes contribute independent temporal variability to sets of single-trial epoch [52]. Figure 11 is an example of ICA in the real world. Figure 12 is the scalp electrodes' locations. Figure 13 is topomap and ERSP for left hand, right hand, foot and tongue imaged movements using ICA spatial filter. Figure 14 is the typical component properties of 4 non-neural ICs such as eye blink, lateral EOG.
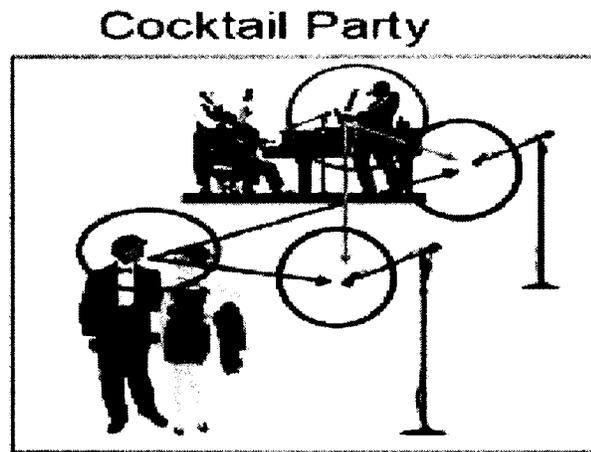
Figure 11: Illustration of ICA in the real world [54].
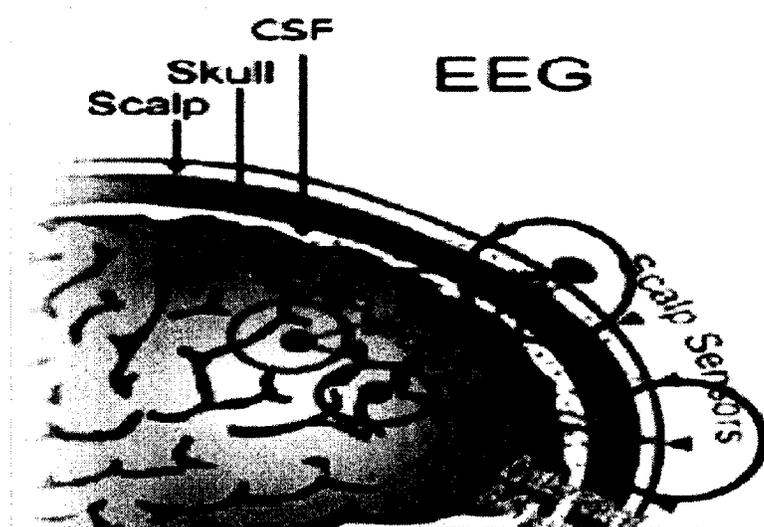
Figure 12: Illustration of signal source location [54].
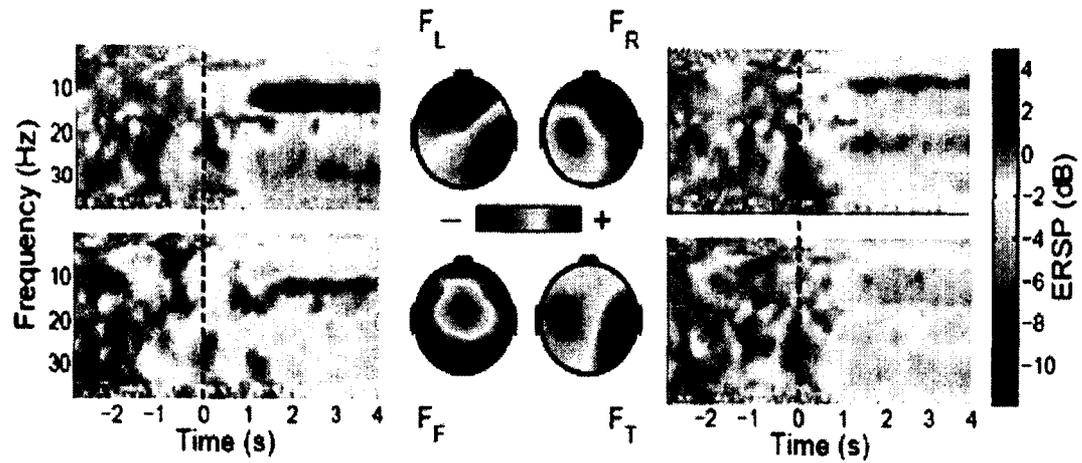
Figure 13: Illustration of topomap and ERSP for left hand, right hand, foot and tongue imaged movements using ICA spatial filter [18].
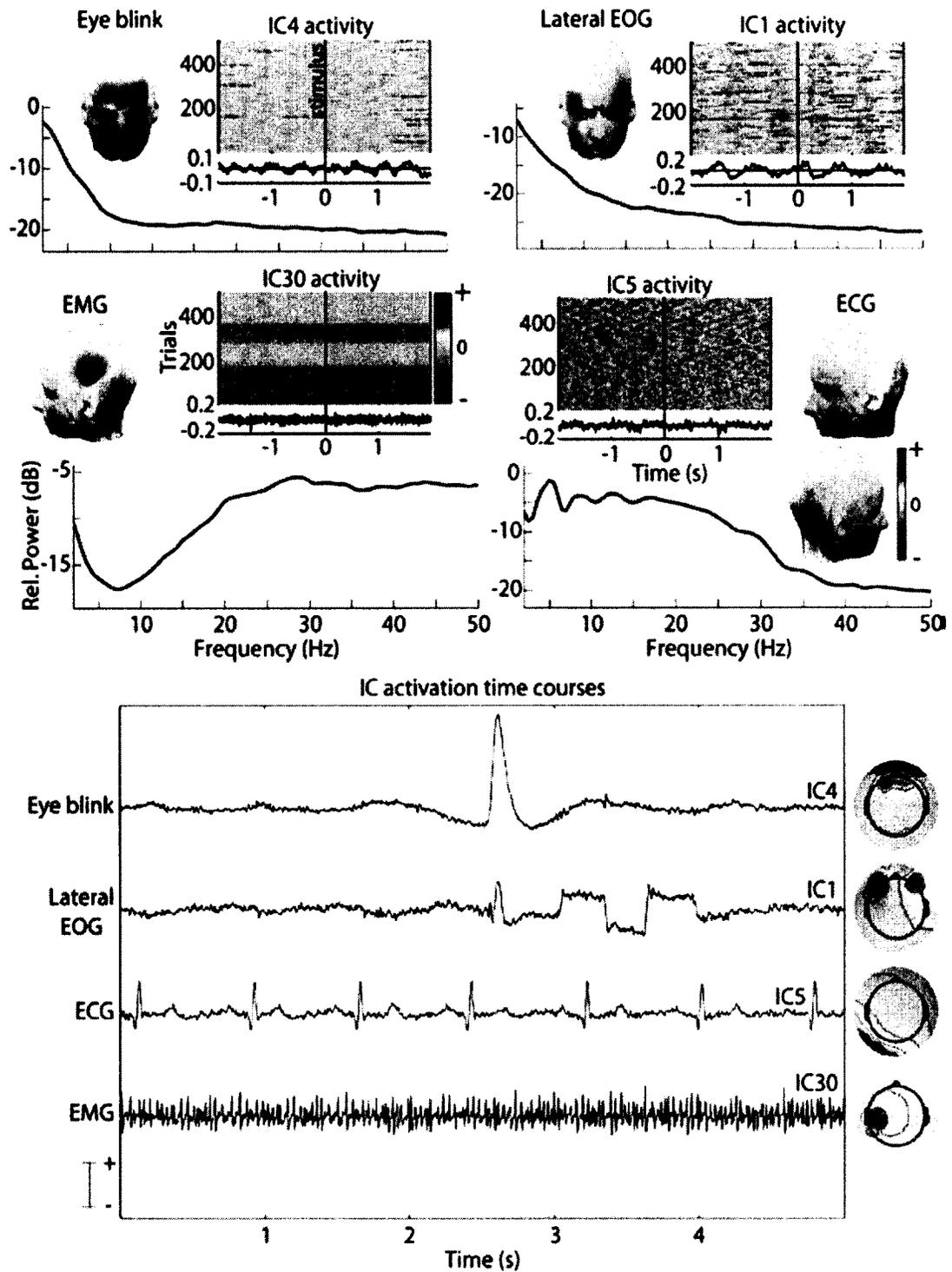
Figure 14: Typical component properties of 4 non-brain ICA such as eye blink, lateral EOG [53].

2.4.2   Empirical Ensemble Mode Decomposition (EEMD)

An empirical mode decomposition (EMD) technique is widely use in signal processing, especially suitable for nonlinear and non-stationary analysis. EMD can decompose the EEG signal into a collection of intrinsic mode functions (IMFs) [55]. IMFs are kind of whole, adaptive and nearly an orthogonal representation of the studied signal [25]. EEMD solves the mode mixing problem utilizing the uniformly distributed reference frame based on white noise. Ensemble EMD enables the EMD method to be a truly dyadic filter bank and in utilizing the scale separation principle of EMD, it represents a major improvement of the EMD method [56]. The EEMD method described some advantages in neurophysiological studies and BCI applications. a) It is usefully in removing artifacts and extracting dependable signal features in high dense array EEG data. b) The EEMD reports for trial-by-trial dynamics to reserve inter-trial variability of periodic activities and investigates the temporary or discontinuous states in neurosignals. c) The effective extraction rate of oscillatory activities can be beneficial for BCI applications. d) The single-trial approach allows an operational in cases where participants can undertake long procedures and in medical settings where patients have attention problems. This approach is capable of sustaining long experiments [57]. Figure 15 is an illustration of EEMD decomposition during the imagination of the combined left-foot with left-hand movement.
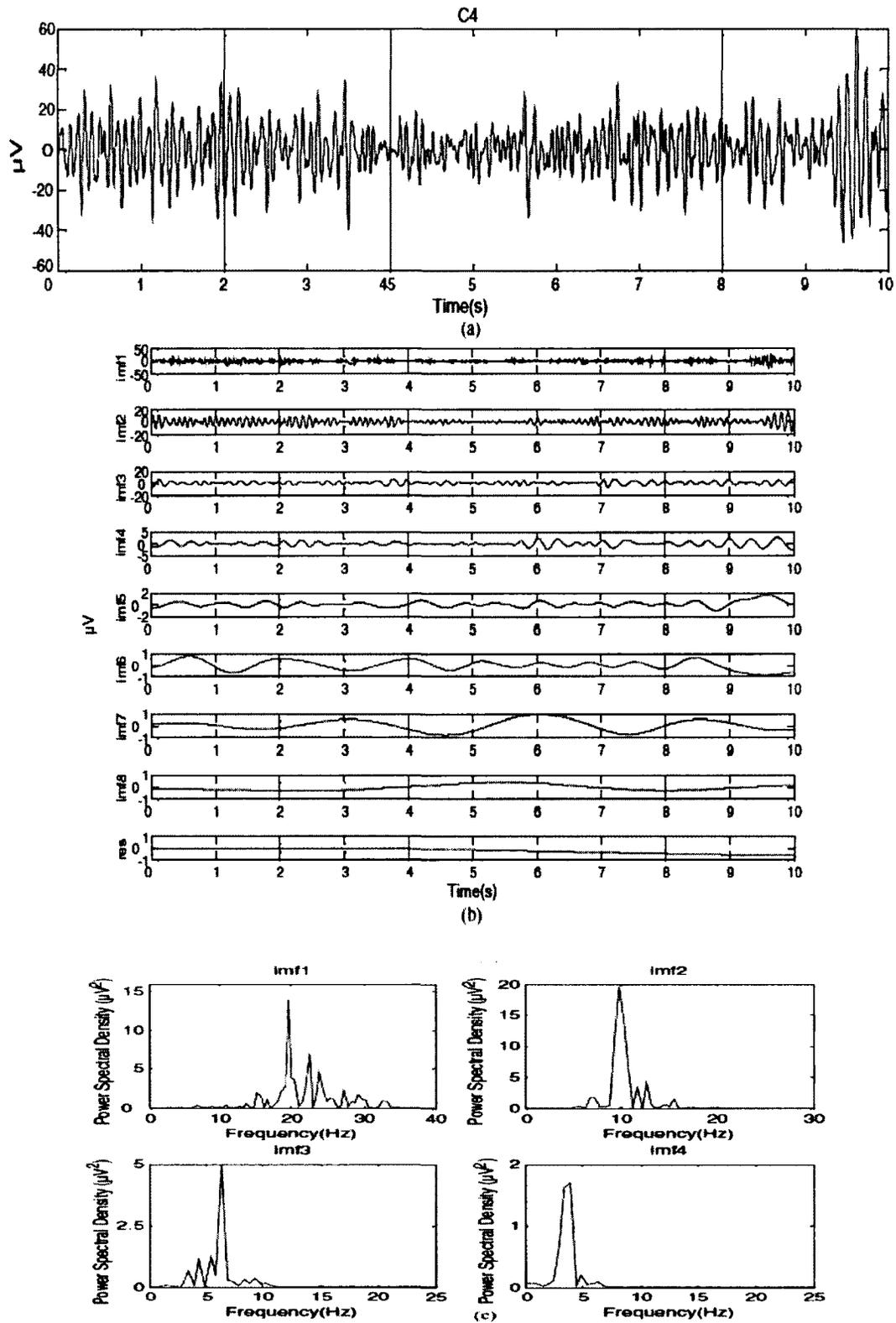
Figure 15: Illustration of the characteristic IMF extraction. (a) The single-trial EEG data at C4 during the imagination of the combined left-foot with left-hand movement. (b) The EMD results of (a). (c) The PSD distribution of the first four IMFs in (b) [25].

2.5   Signal Classification

Fisher's linear discriminate analysis (FLDA) was evaluated in this project. After ICA and EEMD decomposition had been completed, the peak time, active location and frequency content of the directions signal related to the intended arm reaching movement were treated as input vectors of FLDA classifiers. FLDA projects the high dimensional data onto a one dimensional vector. It has a low computational cost, which makes it attractive for real-time implementation. The training process for this method is utilized, averaged, and segmented data from each subject on each experiment date [58]. Figure 16 is the example of FLDA method [59] and Figure 17 is the ICA source localization for classification.
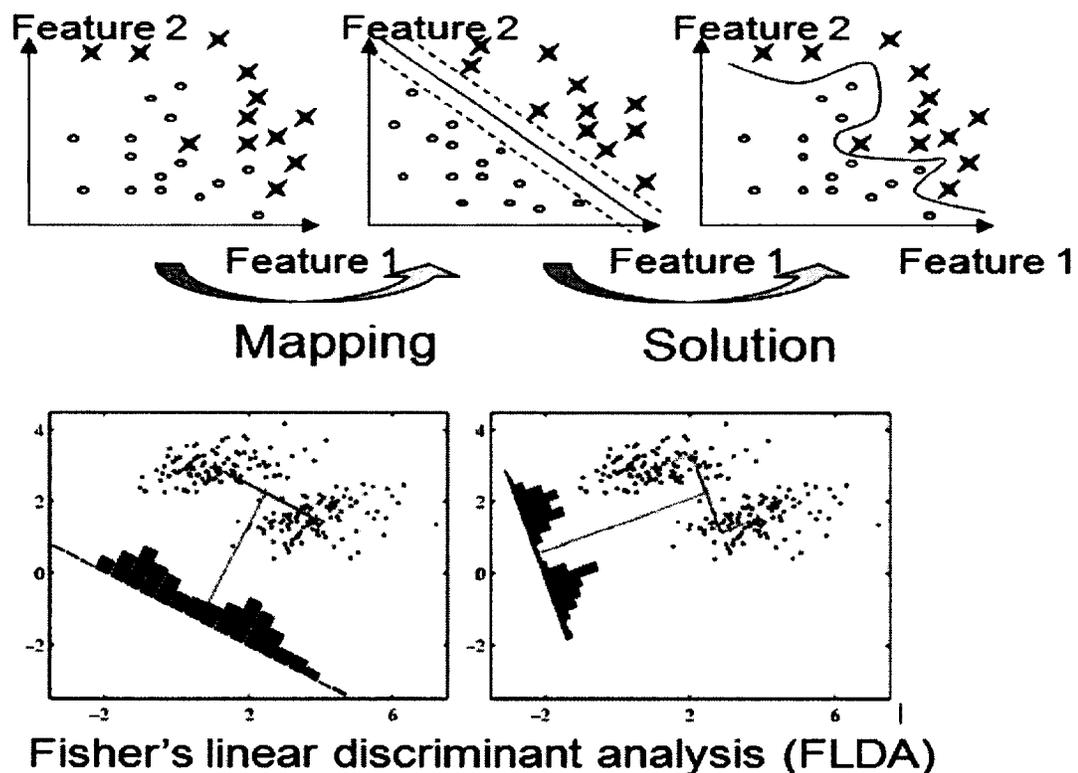
Figure 16: Fisher's linear discriminate analysis [60].

ICA Source Localization for Classification of Mulit-class Intended Hand Movement Tasks
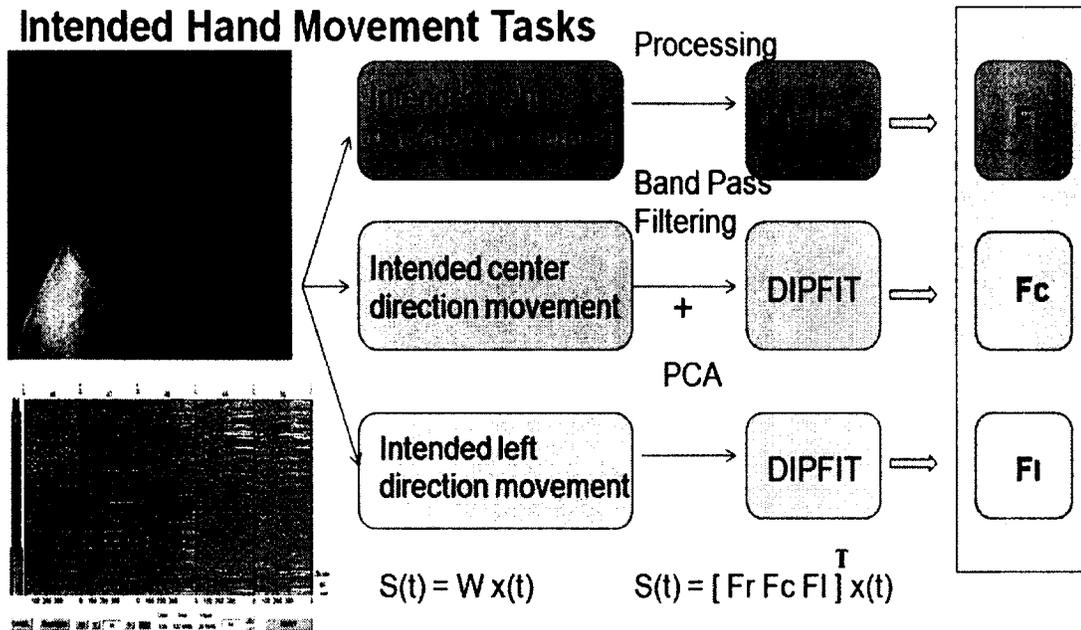
Figure 17: ICA source localization for classification of multi-class intended arm movement.

CHAPTER 3

METHODS

3.1   BCI Based on Motor Intention

The experimental procedure for investigating the motor intention using targeted BCI is shown in Figure 18. It involves the design of a visual stimulation system, an EEG data acquisition system, a signal pre-processing unit, an artifact removal algorithm, a feature extraction method, and a signal classifier. The detail for each step is provided in the subsequent sections. The method for computing the visual-cue based scaling factor is proposed and described in the feature extraction section.
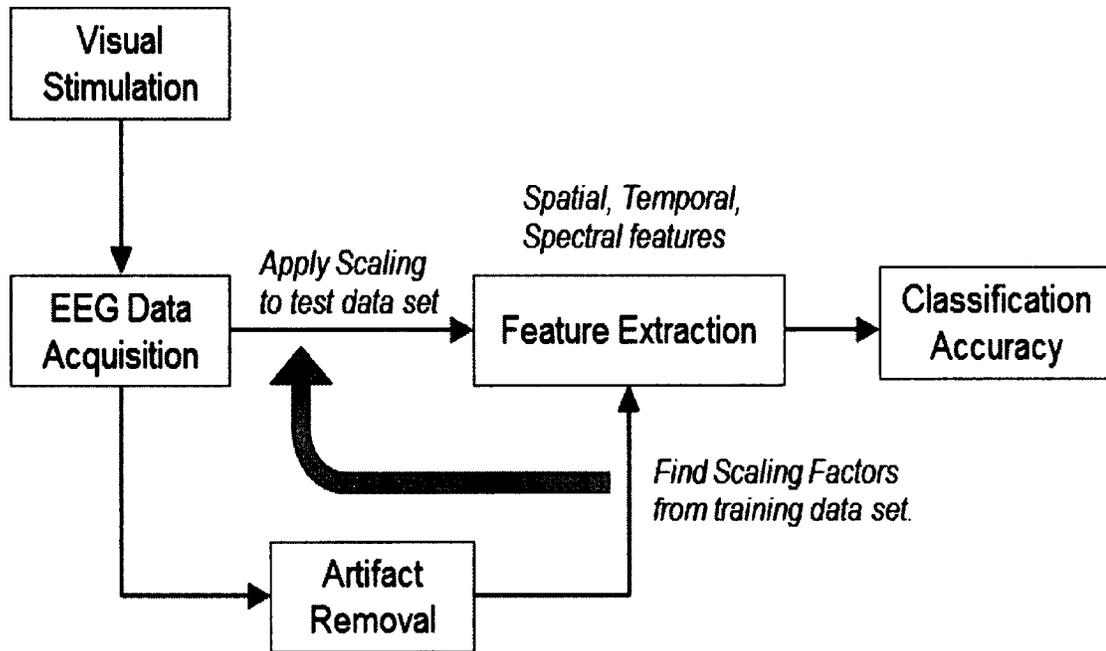
Figure 18: A flow chart describing overall experimental procedure for decoding the reaching tasks during the planning stage. The visual stimulation was provided to subjects for recording EEG signals. Artifact in the data was removed before finding the suitable scaling factors. Once the scaling factors were obtained, they were applied to the signal amplitude features in the test set. To determine the overall accuracy, a 5x5-fold cross validation procedure was performed for a binary classifier.

3.1.1 Visual Stimulation and Data Acquisition

Eight able-bodied participants with normal or corrected to normal eye sight (6 males and 2 females, ages 19-29, all right handed users) were recruited in this study. All of the subjects had no prior experience with BCIs and no history of neurology disorders. The protocol has been approved by the Institutional Review Board for Human Use (IRB) at Louisiana Tech University. All participants had read and signed an informed consent.

The experimental setup is shown in Figure 19 where the subjects were seated in front of a computer screen and given visual cues from the computer monitor. Touch pad sensors were placed at the middle and to the sides of the monitor to track the subject's responses. In order to obtain useful signals for the fast interpretation, the BCI task should

be relatively easy to perform and require little effort from the users to prevent physical or mental fatigue [11]. In order to do so, a targeted delayed saccade/reach task was used in this study. A minimum of 450 trials were performed by each subject. The recording sessions were broken into blocks (90 trials / block), separated by 5 min breaks in between.
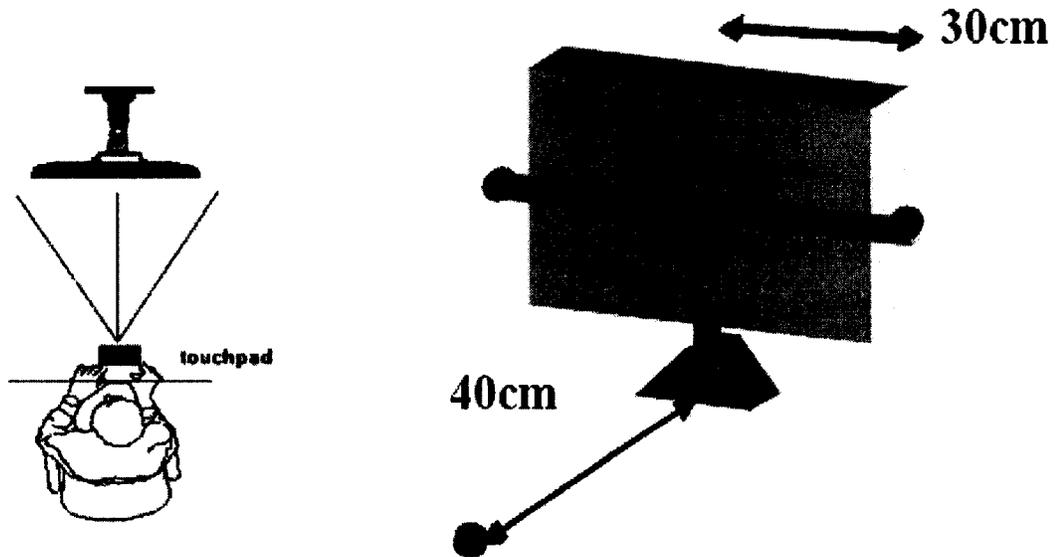
Figure 19: The experimental setup is illustrated. Touch pads (circles) are placed at the base (resting) position and at the targets of the reaching tasks (left, right, and forward) to track whether the subject has performed the tasks correctly.

The sequence of each trial is shown in Figure 20. At the beginning of each trial, each subject was asked to relax the forearm and place the palm on the touch pad at the base position 40 cm away from the screen. Visual cues were provided using the E-Prime 2.0 system (Science Plus Group, Netherland) to inform the subjects of the proper movement to perform in a dark room. Two types of visual cues were provided. First, the "Effector cue" was displayed 500 ms after the beginning of each trial. It instructed which movement type the users should perform (imaginary movement with eyes closed, reach without eye movement, or saccade to target). The second visual cue, called the "Direction cue" was shown at the center of the screen 1000 ms after the "Effector cue". It informed the user of the appropriate reaching directions (left, right, or forward). The subjects were asked to fixate on the center of the screen until the "Go cue" appears 700 ms after the "Direction cue". They were then asked to perform the indicated actions as quickly as possible after the appearance of the "Go cue". The nine different "Effector – Direction" combinations were evenly distributed and randomly provided over the whole experiment. The EEG evoked response potential (ERP) signals were recorded using a 128-channel HydroCel Geodesic Sensor Net (Electrical Geodesics Inc., Eugene, OR) with the Net-Station 5.3 software. Figure 21 shows the electrode placement as viewed from the top of the head and regions of interest around the PPC. All signals were anti-aliasing low-pass filtered at 100 Hz, and digitized at a sample rate of 256 Hz.

Outline of One Trial
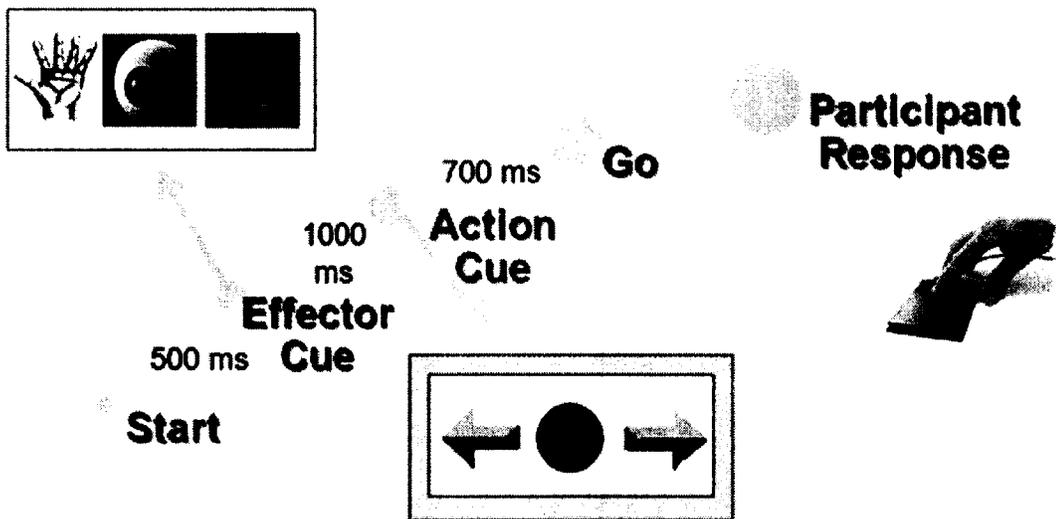
Figure 20: Time course of one trial is illustrated. The 700 ms delay period between the presentation of the "Direction cue" and the "Go cue" is considered the period of directional movement planning. The EEG data within this time window is used for the analysis.

Regions of Interest (ROI)
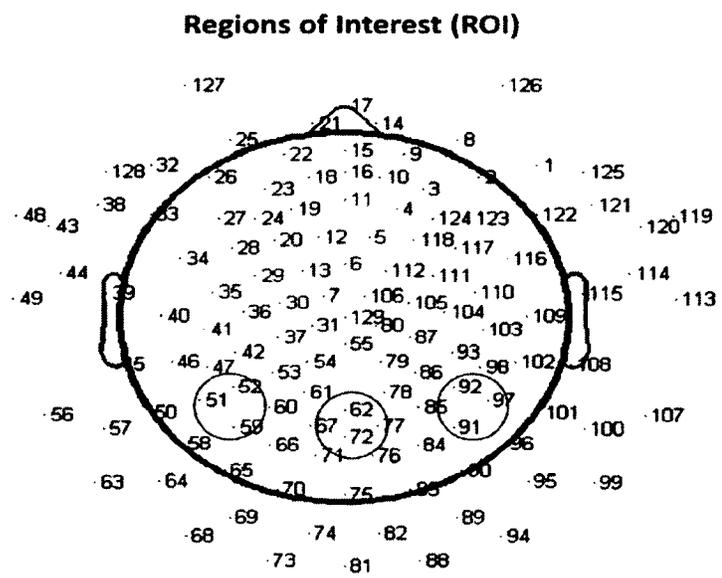
Figure 21: The channel map for 128 electrodes is shown with electrode number labeled. The illustration is observed from the top of the subject's head with the front of the head pointing upward. The regions of interest on the scalp surface near the PPC are circled.

3.1.2 Signal Pre-processing and Artifact Removal

The EEG data was digitally filtered between 0.1~30 Hz. Since this project focused only on the analysis of the motor's intention prior to any actual movements, all three different effectors were included and combined in the analysis. The data was separated into three groups (left, right, or forward) based on the "Direction cues". Bad channels, as the result of poor skin contact, eye blink, eye movement, or muscle movement were detected based on their particular signal characteristics and abnormal amplitude information, were replaced by the averaged signals from neighboring channels using NetStation built-in functions. Only those artifact-free epochs (with amplitude < 50 μV) were used for further analysis. The data was also re-referenced to the average signal across all 128 electrodes. The 100 ms before onset of each trial was also used for baseline correction adjustments.

The average evoked response potentials after the "Action" cue were segmented for analysis (Figure 22). The EEG data from this period represents the planning phase of a motor task, before the subjects were prompted to make any horizontal reaching motions.
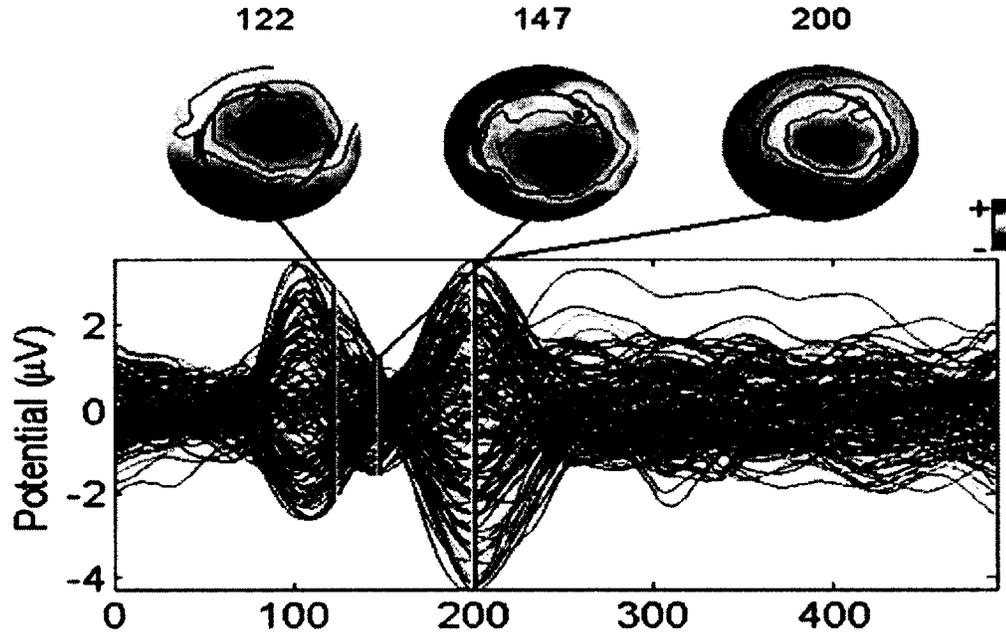
Figure 22: Illustration of surface potential map. The averaged evoked potentials from all 128 channels from one particular subject are shown. The scalp maps at the top represent the spatial activity at a particular time instance that signifies the activation signals in the scalp surface. Specific activities at 122, 147 and 200 ms after the "Action" cue are shown.

3.1.3   Offline Source Localization Validations

Source localization was performed offline as a way to validate that the activated brain regions of our recorded data is consistent with the literature. The process described in this subsection would not be needed in the real-time implementation of the motor intention decoder. Independent component analysis (ICA) [61] was first performed using the extended Infomax-ICA algorithm in the EEGLAB tools [53] to find the maximally, temporally independent signals available [62]. Independent components (ICs) related to motion artifacts can be identified visually based on the spatial contribution of each IC. We have used ICA to effectively detect, separate and remove activity in EEG records from a wide variety of artifactual sources (Figure 23). Figure 24 illustrates the averaged

signals across all the recording trials before and after the removal of eye motion artifact.

The DIPFIT 2.0 algorithm was then used to estimate the dipole sources of the remaining

independent component (IC) after spatial filtering [53]. The dipoles were projected onto

the boundary element mode in EEGLAB, then plotted on the average MNI (Montreal

Neurological Institute) brain images [63]. The source locations were then specified using

the Talairach coordinate system. Dipole locations from the source localization algorithm

would not be used in the single-trial classification of arm movement direction since it is a

time consuming process.
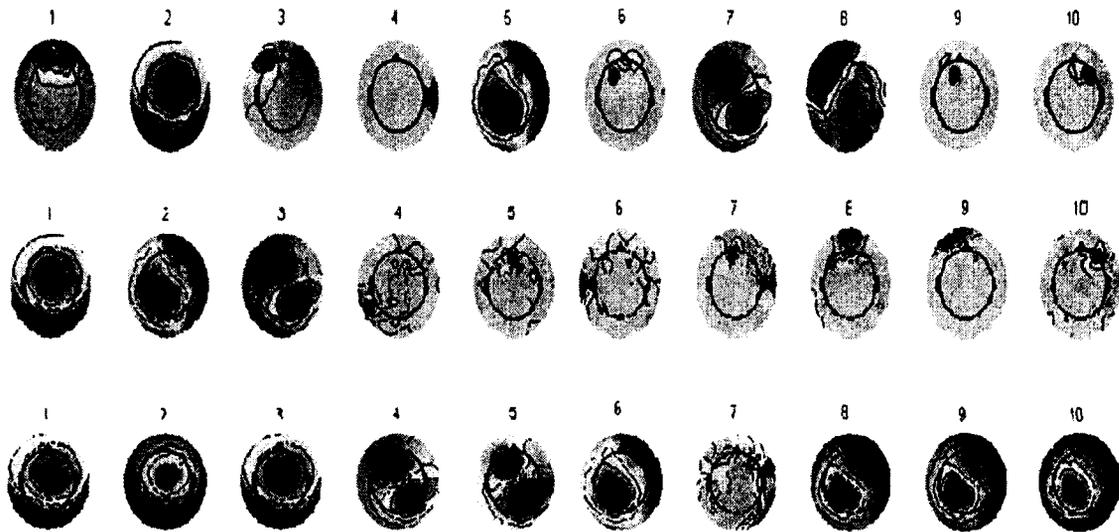
Figure 23: The projection of each independent component. The ten largest identified ICs at different stages of the ICA pruning process are shown. (Top row) The original ICs after the first ICA. Lateral eye movement artifacts are shown in IC#1, 3 and 6. Muscle artifacts are shown in IC#2 and 4. (Middle row) After the first pruning process, ICA was run again. Here, the ICs corresponding to the left and right movements are more apparent at IC# 2 and 3. (Bottom row) After the second pruning step, 9 out of 10 components shown are related to the intended arm movement.
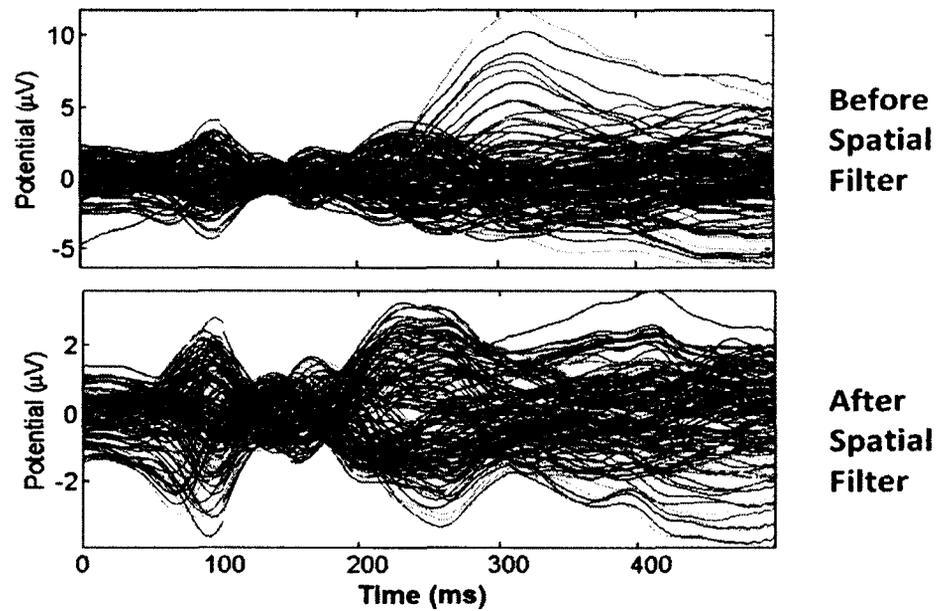
Figure 24: EEG signals before and after spatial filtering is shown. The signal for each channel is averaged across all trials prior to ICA spatial filtering. An example of eye artifact is seen in the EEG spatial map around 305ms. After eye artifact is removed, the averaged signal for each channel after ICA spatial filtering is shown at the bottom subplot.

3.1.4   Ensemble Empirical Mode Decomposition

Ensemble empirical mode decomposition (EEMD) is a data-driven analysis method that separates the signal into a collection of intrinsic mode functions (IMFs). It is a powerful approach for analyzing nonlinear, non-stationary EEG signal since the method is only based on the local characteristic time scale [55-57]. Unlike traditional bandpass filters, EEMD breaks down the signals in an empirical manner, which is strictly based on the signal characteristics without specifying any frequency bands [64]. Mode mixing problem that existed in the Empirical mode decomposition (EMD) method can be resolved by EEMD utilizing the uniformly distributed reference frame by the addition of white noise [65]. The procedure for EEMD has been described in great detail in [56], and would not be repeated here.

3.1.5   Feature Extraction and Signal Classification

Signal classifiers were created using the Statistical Pattern Recognition Toolbox in Matlab [66] to decode the EEG signal features. A two-class analysis (left versus right) was first performed using Fisher Linear Discrimination (FLD) binary classifier in a 5x5-fold cross validation procedure. Eighty percent (80%) of the data for each direction was randomly chosen to be the training set. The remaining 20% of the data was assigned to be the testing set. The "signature" signal was acquired in each region of interest (ROI) near the PPC region (see Figure 21) using the training set for each cross-validation study. In this study, the averaged ERP signal within 235 ms after the presentation of the "Direction cue" would be considered the "signature" at each ROI. It has been observed that regardless of the intended reaching direction or the type of effectors requested of the subject, the averaged EEG signal within the first 235 ms after the presentation of the "Direction cue" retains a similar signal profile. Each "signature", consisted of a dominant high delta (0 – 4 Hz) and a low theta (4 – 8 Hz) component, has been observed to have similar shapes, regardless of the intended direction of movement. The local maximum and local minimum of the "signature" signal at each ROI were found and their difference was used as a scaling factor. The signal amplitude at each recording site was scaled accordingly with the following equation:

$$v_{i,scaled}\left(t\right) = \frac{v_i\left(t\right) - v_{i,min}}{v_{i,max} - v_{i,min}} \qquad \text{Eq. 1}$$

where $v_i(t)$ and $v_{i,scaled}(t)$ denote the ERPs in the test set, at location i, before and after scaling. The values $v_{i,max}$ and $v_{i,min}$ are the maximum and minimum of the "signature" at the same location, found in the averaged training data set. Since this scaling process only

involves multiplying the EEG recording by a different factor at each location, it is suitable for real-time applications. Figure 25 is the graphical illustration for scaling the EEG signals.
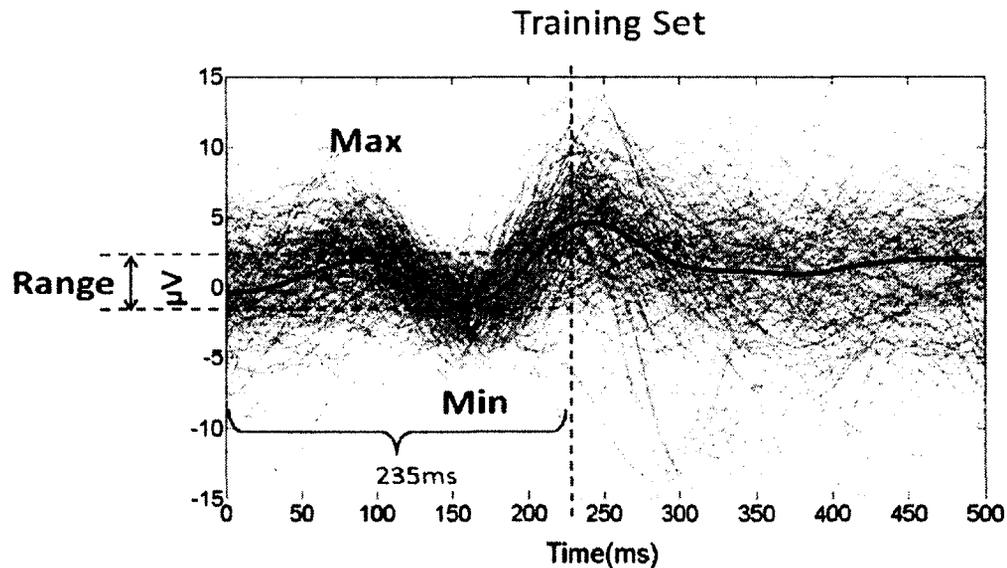
Figure 25: Graphical illustration of the scaling factor is shown. The scaling factor computed from the individual recording channels in the training set is applied to the test set before signal classification. The light color lines indicate the EEG signals at a single electrode from different trials in the training set; the dark bolded line indicates the average signal at that particular electrode location. The scaling factor is set to be the difference between the maximum and minimum values in the first 235 ms of the averaged signal.

The impact of scaling was evaluated by investigating the features at different time delays after the "Direction cue" [67]. Once it has been established that using this cue-based "signature" can enhance the binary classification accuracy of the planned motor movement in two directions, we performed the second analysis. It involved the evaluation of the EEMD-based operation on the decoding accuracy. The high frequency noise in the EEG data was reduced through the elimination of IMF1 and IMF2 [68], since the ERP difference of intended direction of movement have been reported to be < 12 Hz [69].

3.2   BCI Based on Visual Working Memory

The experimental procedure for investigating the visual working memory using electrophysiological and behavior evidences is shown in Figure 26. It involves an EEG data acquisition system, a signal pre-processing unit, an artifact removal algorithm, ANOVA method, and time-frequency analysis. The detail for each step is provided in the subsequent sections below.

```
┌──────────────────┐          ┌──────────────────┐
│   EEG raw data   │ ───────▶ │ ICA decomposition│
│   (128-channel)  │          │     (EEGLAB)     │
└──────────────────┘          └──────────────────┘
         │                             │
         ▼                             ▼
┌──────────────────┐          ┌──────────────────┐
│  Time-Frequency  │          │    Correction    │
│ Analysis and     │          │       for        │
│    statistics    │          │     artifacts    │
└──────────────────┘          └──────────────────┘
                                       │
                                       ▼
┌──────────────────┐          ┌──────────────────┐
│      ANOVA       │ ◀─────── │       ERPs       │
│   On ERPs data   │          │   (0.1-80Hz)     │
└──────────────────┘          └──────────────────┘
```
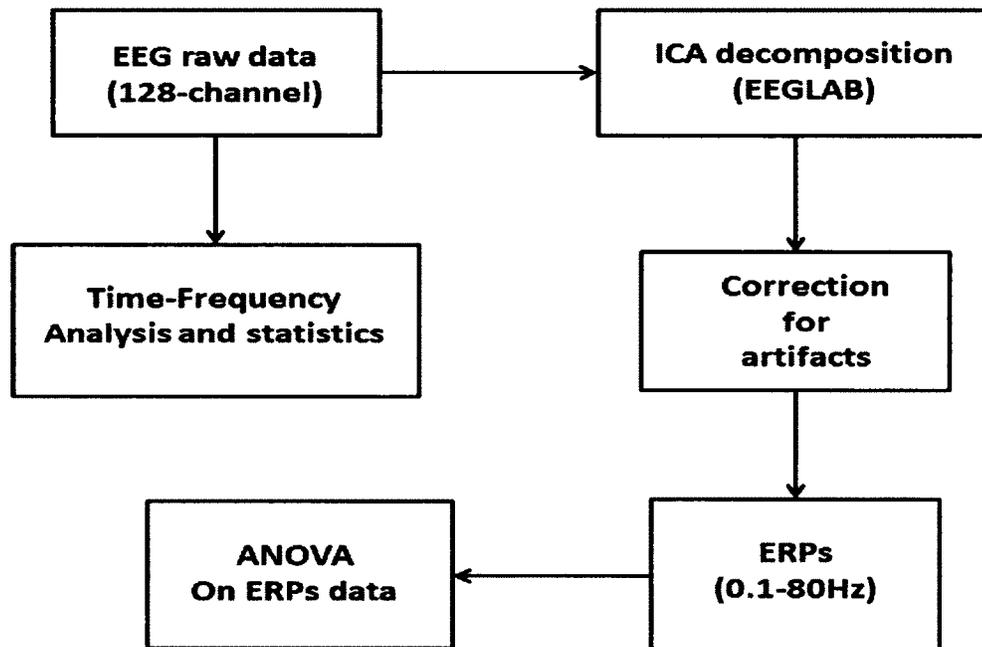
Figure 26: A flow chart describing overall experimental procedure for visual working memory data analysis.

3.2.1   Visual Stimulation and Data Acquisition

Sixteen healthy, young participants (18-31 years of age, 5 females and 11 males) performed the VWM load tasks: two of the subjects participated in the training gains study, and four individuals completed the transfer benefit tasks (two people per training and control group). All participants had normal or corrected to normal eye sight. None of them have a reported history of neurological or psychological disorder. All of them had

no prior experience with computerized VWM training. The experimental protocols were approved by Louisiana Tech University's Institutional Review Board Committee. All participants gave informed consent. The experimental data from one of the participants was rejected from VWM load experiments due to an excessive amount of bad trials (> 30%) related to eye movement or eye blinks.

Participants were seated in front of a computer screen and given visual cues at a distance of 80-100 cm in a dark sound-attenuated room. They were instructed to respond to the VWM arrays by pressing a button on a response pad and performing as quickly and accurately as possible to the assigned tasks. All experiments were conducted between 9:00 am and 1:00 pm. Each subject was only given 10-20 min of practice time before the start of the VWM load tasks.

The sequence of each trial for the VWM load and training gains experiments (change-detection: color and position) is shown in Figure 27A. At the beginning of each trial, a central arrow cue instructed the subjects to focus on either the left or right hemi-field for 500 ms. Memory arrays were displayed as 2, 4, 6, or 8 colored squares consisting of 2-9 possible colors (red, blue, black, yellow, green, purple, gray, orange, and light blue) on each side of a central fixation cross for 100 ms. The color of each square was randomly chosen one at a time (no repetitive color appeared in the same memory array on each side). The positions of colored squares were also randomly arranged in each trial. Fifty percent of the trials had the same colored and oriented squares in both memory and test arrays. Another fifty percent of the trials presented different targets in the test array. Each memory and test array pair was separated by a 900 ms retention interval. The test array would last, at most, 2000 ms, or until a subject

responded. A 500-ms inter-trial interval would directly follow the termination of the test array.

The transfer benefit tasks (Figure 27B.) not only asked the observers to memorize the feature characteristics of the items in the memory arrays (change-detection: color, position, and shape), but also the location of a particular item displayed in the test array. Participants in the training group before and after the VWM training gains experiments were labeled as TB1 and TB2, respectively. For comparison, the control group was assigned to include the participants with data recorded only at the beginning and at the end of a 12-week period, without any training sessions in between. In order to reduce user fatigue, the recording sessions were separated into blocks with 5 min breaks. Depending on the experiment, each block consisted of 100 trials of VWM load experiment, 150 trials for training gain, or 150 trials for transfer benefit experiments. Consequently, the VWM load task was divided into 6 blocks, the training gain and transfer benefit tasks were separated into 4 blocks, with each block lasting approximately 10 min. The total experiment time required for each day was about 2 hr.
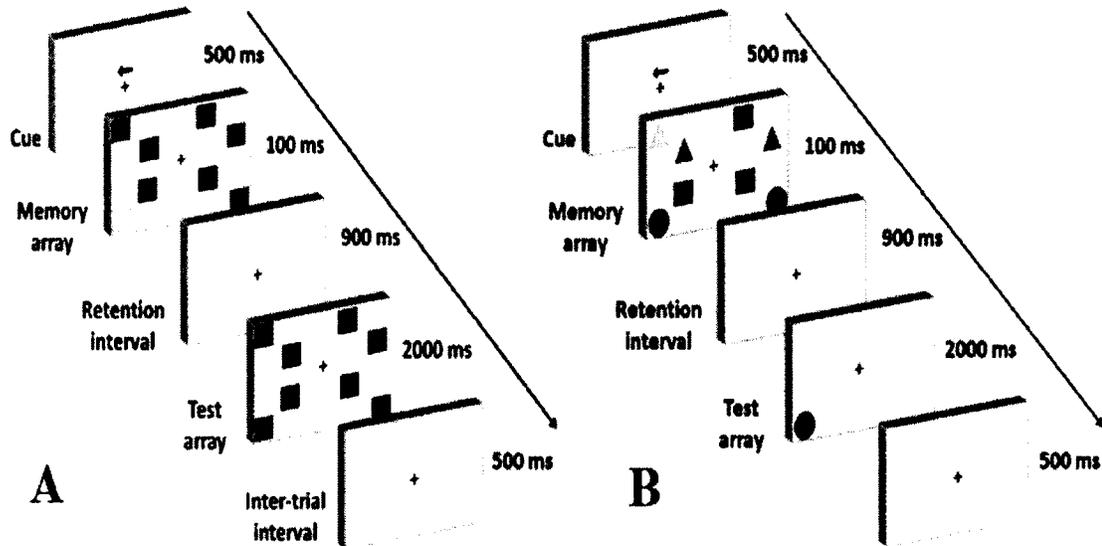
Figure 27: Example of a visual working memory trial for the left hemi-field. A. The VWM load and training gains experiments are easier to detect a change where the position context is the same in both memory and test arrays. B. The transfer benefits experiment not only asked the observers to memorize the feature characteristics of the items in the memory arrays (colors, positions and shapes), but also where the position was altered in the test array.

Electroencephalogram (EEG) evoked response potential (ERP) signals were recorded using a 128-channel HydroCel Geodesic Sensor Net (Electrical Geodesics Inc., Eugene, OR) with Net-Station 5.3 software. Regions of interest (ROI) around the posterior parietal cortex (PPC) were selected from the following standard international 10/20 posterior parietal electrodes for P3, P4, P5, P6, PO5, PO6, O1, O2, T5, and T6. All signals were anti-aliasing, low-pass filtered at 100 Hz, and digitized at a sample rate of 250 Hz.

3.2.2   EEG Preprocessing and Artifact Removal

The EEG data were digitally filtered between 0.1 ~ 30 Hz. The data were segmented into individual groups based on the number of items in the memory array. Each data segment, or epoch, lasted 1200 ms, and consisted of a 200 ms pre-memory array, a 100 ms memory array, and a 900 ms retention interval. The epochs of poor skin

contact, eye blink, eye movement, or muscle movement were detected and removed based on their particular signal characteristics and abnormal amplitude ($\pm$ 25 μV) using EEGLAB [53]. Approximately, 15-20% of the trials were rejected based on the above criteria. Only eye blinks and horizontal eye movement were removed through independent component analysis (ICA) with topographies [70], resulting in 20-25 independent component removals [71]. The data were also re-referenced to the average signal across all 128 electrodes. The first 200 ms of each trial was used for baseline correction adjustments.

ERP waveforms were obtained from posterior parietal cortex over selected latency ranges (1200 ms). The P1 wave was identified as the first positive peak after the memory array cue during the 50-100 ms time window. The N1 wave was defined between 100-180 ms [31]. Trials were averaged into segmented grand average ERPs for each participant. CDA (300-1000 ms) was measured as the ERP amplitude from electrodes contralateral to the location of the task-relevant cue in the memory array [72]. We used the results from T5/T6 because the CDA amplitude was consistently higher. However, the same patterns can be obtained over P3/P4, P5/P6, PO5/PO6, and O1/O2 electrode pairs [73].

3.2.3 Behavior Measures

For each participant, the reaction times (RT) were calculated regardless of the correctness of the subject responses. A default RT of 2000 ms was used if the subject did not respond. The mean RT value from the result is different from other studies which only included correct-responses [74]. Accuracies in percent correct responses were calculated from all recorded trials.

3.2.4   VWM Capacity

The formula developed by Cowan was used to estimate the VWM capacity [75]. $K = S*(H-F)$, where K is the memory capacity, S is the item in a memory array, H is the hit rate, and F is the false rate. Generally, the working memory was considered to have a limited capacity. The assumption was that an observer can hold K index in memory from S items in the memory array, guided by the correct performance on the VWM experiments. This formula adjusts the false rate to correct guessing. The commonly accepted capacity limit for an individual is four items.

3.2.5   Statistical Analysis

One-way ANOVA statistical analysis [76] was performed to compare the VWM capacity and average CDA amplitude in each individual. A value of $p < 0.05$ was accepted as significant. All values are expressed as mean ± standard error (Mean ± S.E.).

CHAPTER 4

RESULTS

4.1   BCI Based on Motor Intention

Using the Talairach coordinate system, the dominant equivalent dipole source for each intended arm movement direction was observed near the PPC areas for all subjects. Figure 28 illustrates the result of the EEGLAB plug-in DIPFIT2.0 output for a particular subject where the coordinates for the left component [-20, -40, 24], the forward component [0, -33, 40], and the right component [28, -40, 23] are found. This is consistent with the results reported in the literature [13]. The effects of the parietal ICs were then back-projected onto the scalp for each subject after artifact removal (Figure 29).

Figure 28: Source reconstruction for three equivalent dipoles is illustrated. As a validation, estimated source dipole locations were found to be near the PPC regions, consistent with reported literature [2] with the residual variance for each dipole estimate found to be < 6%.
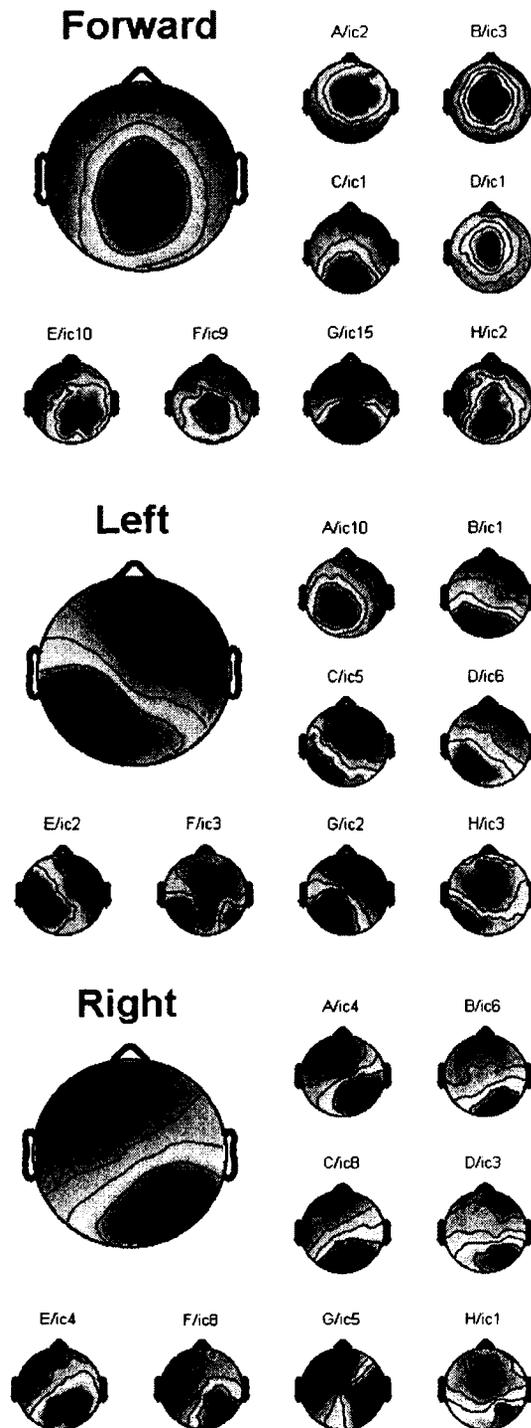
Figure 29: The independent component (IC) clusters of each subject are shown. The three ICs clusters that extracted from eight subjects' ICA decomposition demonstrate activities at posterior parietal cortex region. The larger heads show the average projection across eight subjects. The smaller scalp maps are from individual subjects.

The evaluation of the EEMD-based operation on the decoding accuracy was performed by comparing the FLD decoder performance on IMF-removed data set. Since the average EEG signal amplitude in a 40 ms window was the feature of signal, removing IMF1 and IMF2 components did not significantly improve the decoder performance from $93.91 \pm 6.09\%$ to $95.44 \pm 3.28\%$ ($p > 0.4$).

As a preliminary evaluation of the proposed cue-based scaling strategy, a two-direction (left versus right) classifier was created. The averaged ERP data from the training set at each recording site was found, the scaling term was calculated to be the difference between the maximum and minimum values within 235 ms after the presentation of the visual cue. Once the scaling factors were found, they were applied to the test set. Amplitude features at different time delays were evaluated and the improvement of classification accuracy after the scaling operation is shown in Figure 30. The highest classification accuracy (on the scaled data) was found to take place 271-310 ms after the visual cues. Statistically, significant improvement ($p < 0.01$) in classification performance was found with scaling (accuracy $93.91 \pm 6.09\%$) than without (accuracy $60.11 \pm 9.02\%$). Table 1 summarizes the subject-by-subject result for the single-trial FLD using 5x5-fold cross validation. Figure 31 is shows the scatter plot of EEMD-based features for left and right intended movement separated by FLD classifier.
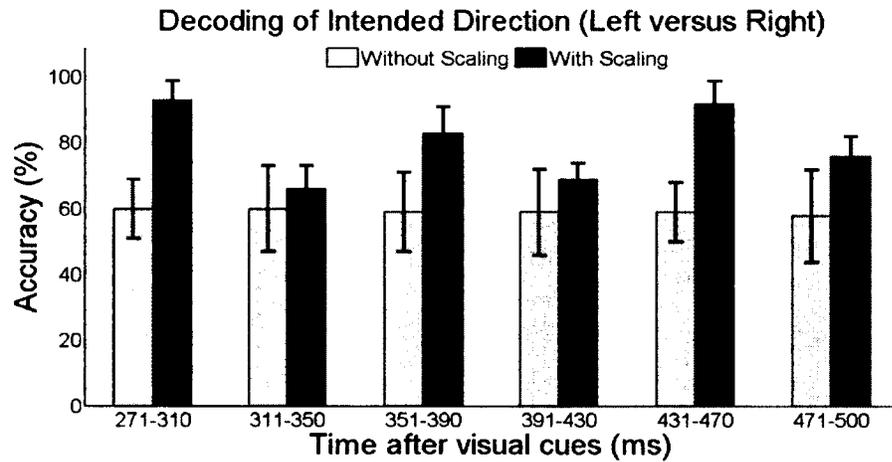
Figure 30: EEG amplitude features obtained in the PPC regions can be used to classify the intended direction of reaching motion. Classification accuracy is at the highest using amplitude features 271-310 ms after the presentation of the visual cues.

Table 1: Single-trial binary classification of left versus right intended movement was performed using FLD. Statistically significant improvement in accuracy was found after cue-based "signature" scaling (p < 0.01).

Subject	Without Scaling Mean ± Stdev	With Scaling Mean ± Stdev
A	66.40 ± 8.11%	99.33 ± 0.83%
B	59.20 ± 4.05%	96.13 ± 3.87%
C	72.80 ± 5.68%	91.60 ± 4.89%
D	55.23 ± 5.48%	96.80 ± 2.25%
E	68.54 ± 4.91%	95.33 ± 2.50%
F	57.67 ± 5.49%	78.71 ± 7.03%
G	54.75 ± 5.37%	94.79 ± 2.31%
H	46.29 ± 5.54%	98.58 ± 1.43%
Mean ± Stdev	**60.11 ± 9.02%**	**93.91 ± 6.09%**
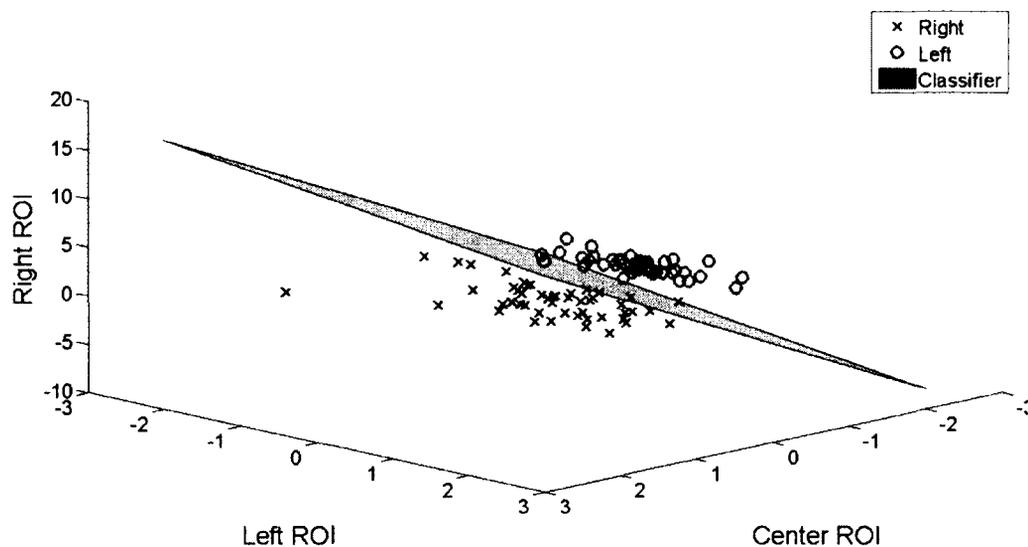
Figure 31: Scatter plot of EEMD-based features for left and right intended movement separated by FLD classifier.

4.2 BCI Based on Visual Working Memory

4.2.1 4.2.1 VWM Load Experiment

The goal of the VWM load experiment was to estimate the VWM capacity. Because the information that can be maintained and stored in memory is limited, it is important to understand the individual differences that may impact one's ability to learn. Behavior and brain activity could predict the VWM capacity by high accuracy and the level of amplitude [77, 78]. This VWM load experiment also included a parametric manipulation of the number of possible items in the memory array to further test the hypothesis that CDA amplitude can be used to understand the VWM templates [73, 79]. The ERP waveform amplitudes and memory capacity were compared. Also, the reaction time (RT) and CDA amplitude were measured at different levels of memory load.

The average accuracy decreased significantly as the number of items increased the conditions (96.46 ± 0.85%, 90.27 ± 1.51%, 77.5 ± 2.35% for 2-, 4-, and 6-items, respectively; p < 0.005) as indicated in Figure 32A. A large drop in accuracy for 6-items

suggested that memory array of this complexity may have exceeded the individual's memory limit. The overall capacity was 2.8 items for 15 participants. Even though this value is smaller than the reported maximum "magic number 4" [75], it still falls within the range of the lateral effects for similar experiments [77]. Nevertheless, the reaction time was significantly slower from 2- or 4- to 6-item conditions (570.3 ± 24.7 ms vs 579.5 ± 22.2 ms vs 648.1 ± 31.6 ms, respectively; $p < 0.05$). The reaction time was highly affected by the difficulty of memory array in Figure 32B.
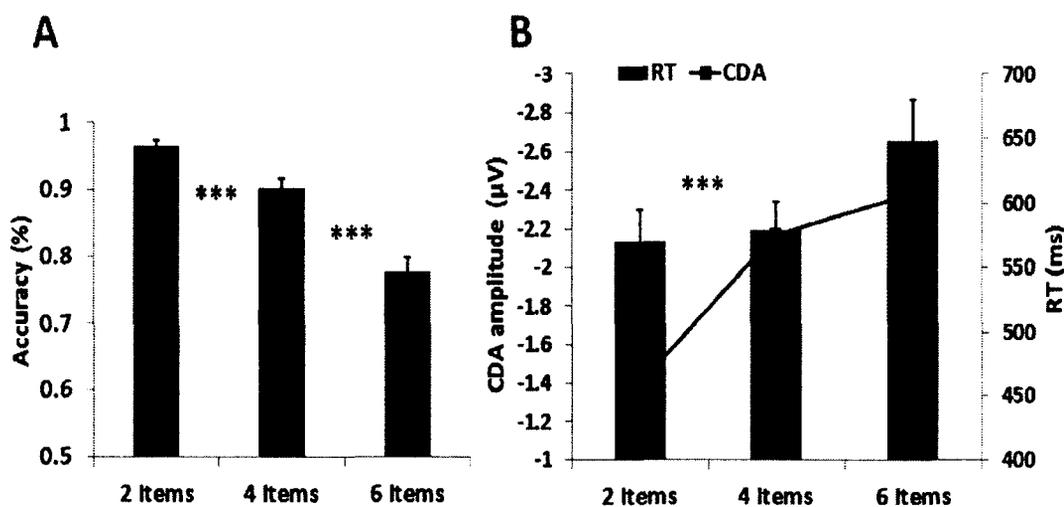
Figure 32: A. The average accuracy across 15 participants for 2-, 4-, and 6-item conditions. B. Combined RT and CDA results. Bar graph (right-axis), RT. Line graph (left-axis), CDA amplitude. Error bars represent confidence intervals. *** $p < 0.005$ for comparisons between adjacent conditions in A and between mean CDA in B.

Figure 33A shows the average waveforms from the posterior parietal electrodes contralateral to the location of the cue for each trial of the VWM load experiments. The CDA components during the time duration 300-1000 ms after the memory cue were measured and indicated by the gray shaded region. A paired comparison of the mean CDA showed a significant increase from the 2- to 4-item condition ($-1.40\mu V$ and $-2.17\mu V$, respectively, $p < 0.005$), while no significant difference was evident between 4-

and 6-item conditions (-2.17µV and -2.38µV, respectively, p > 0.05). This provided

statistical evidence that the CDA reaches a plateau at approximately 4 items which was

the suggested maximum memory capacity for most people [80]. The largest ERP

amplitudes were found at the posterior lateral parietal electrode sites at the latency of

mean N1 peak (100-180 ms) [81] as shown in Figure 33B.
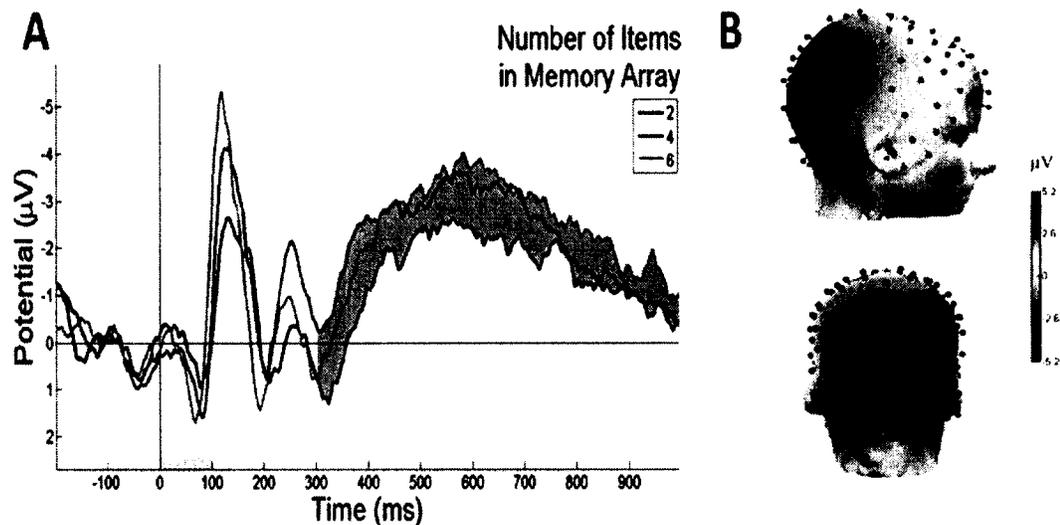
Figure 33: An electrophysiological summary of the VWM load experiment result is shown. A. The grand average ERP waveforms of 15 subjects (from T5/T6 electrodes), contralateral to the location of the cue during the stimulus encoding phase are shown. The gray shaded region indicates the duration (300 - 1000 ms after cue onset) in which the CDA components were measured. The yellow bar (0 - 100 ms) on the timeline represents the epoch of the memory cue. B. The scalp topographies of the VWM load experiments at the latency of mean N1 peak (100–180 ms) illustrate activated posterior parietal regions.

CDA can be used to measure the number of items represented in the memory

array; therefore, a relationship between CDA and the efficiency of the VWM response

can be found (Figure 32B). As expected, an increase in RT corresponds to increased

difficulty in the memory array. Likewise, the CDA also demonstrated this similar trend in

which CDA positively correlates with the memory capacity for 2-, 4-, and 6-items (r =

0.36, 0.42, and 0.61, respectively, p < 0.005) (Figure 34). Therefore, individuals with low memory capacity depend on more working memory to perform VWM load tasks. In contrast, participants with high memory capacity could perform VWM tasks much more easily and efficiently. Likewise, they are able to process and store higher amounts of information during the VWM load experiments. The relationships among CDA and RT and memory capacity is critical in revealing a strong link between the behavior and neural evidence.
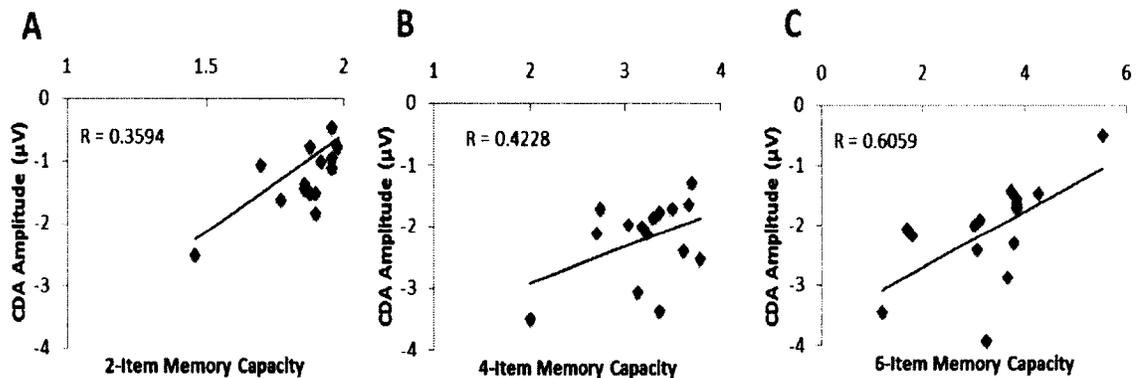
Figure 34: The combined behavioral and electrophysiological summary of the VWM load experiment. A-C. Memory capacity and CDA amplitude demonstrate linear correlations in the 2-, 4-, and 6-item conditions.

4.2.2   VWM Training Gains Experiment

The goal of the VWM training gains experiment was to develop VWM training procedures that would lead to general cognitive improvement. Increase in behavioral accuracy and brain activity is the marker of improved performance, because it was highly related to the reaction time, VWM capacity, and CDA amplitude in Figures 32B and 34. We compared the difference in training gains for various levels of difficult tasks where CDA changes can be considered as a predictor of memory capacity improvement.

VWM training gains within the 12-week intervention period are shown in Figure 35A. At the beginning of the training gain tasks (1st week), the average accuracies of the 8-, and 6-item conditions were 62.67% and 83%, respectively. An accuracy exceeding 93% was found in the 4- and 2-item conditions. After 12 weeks of training, participants achieved significant improvements in the average accuracies (up to 87.67%, 94.67% and 99.67% for the 8-, 6- and 4-item trials, respectively). Since there was a high baseline level in average accuracy (98 - 100%) for the 2-item trials, no significant difference was found after 12 weeks of training. Specifically, there were two significant drops in the 4th and the 9th week in the 6-item condition, possibly caused by the subject's loss of attention during this long training period. However, the overall VWM performance demonstrated an increasing trajectory from week to week. This result indicates that memory capacities of individuals have already shifted to the upper-limit level, which also means that the VWM capacities of the trainees have expanded through a long period of training. Consequently, Figure 35B shows that the reaction time has speeded up after 12 weeks of training in all 2-item, 4-item, 6-item, and 8-item conditions (570 ms vs. 478 ms, 613 ms vs. 524 ms, 699 ms vs. 578 ms, and 751 ms vs. 563 ms), which suggests that the participants felt more confident performing tasks in the last week than the first week.

The average N1 amplitude (100 - 180 ms) and CDA amplitude were significantly lower in the 2-item trials than the 4-, 6-, and 8-item trials during the first two weeks, as shown in Figure 35C (-1.89 µV, -3.01 µV, -3.53 µV, and -4.00 µV, respectively; $p < 0.005$). This relationship is consistent with the VWM load experiment at the maximum memory capacity of 4-items. The average CDA increased as the difficulty level increased. This situation was observed only in the early training period. This implied that

the subjects had to pay more attention to the more difficult tasks, such as 4-, 6- and 8-item trials, as the ERP waveforms were modulated by attention [82]. However, with continual regular training, the average CDA changed gradually over time, resulting in negligible difference between the CDA patterns for the 2-, 4-, 6-, and 8-item conditions (-2.37 μV, -2.22 μV, -2.13 μV, and -2.56 μV, respectively; $p > 0.05$), as shown in Figure 35D. This might be due to the fact that the participants' VWM capacities were enhanced by training.
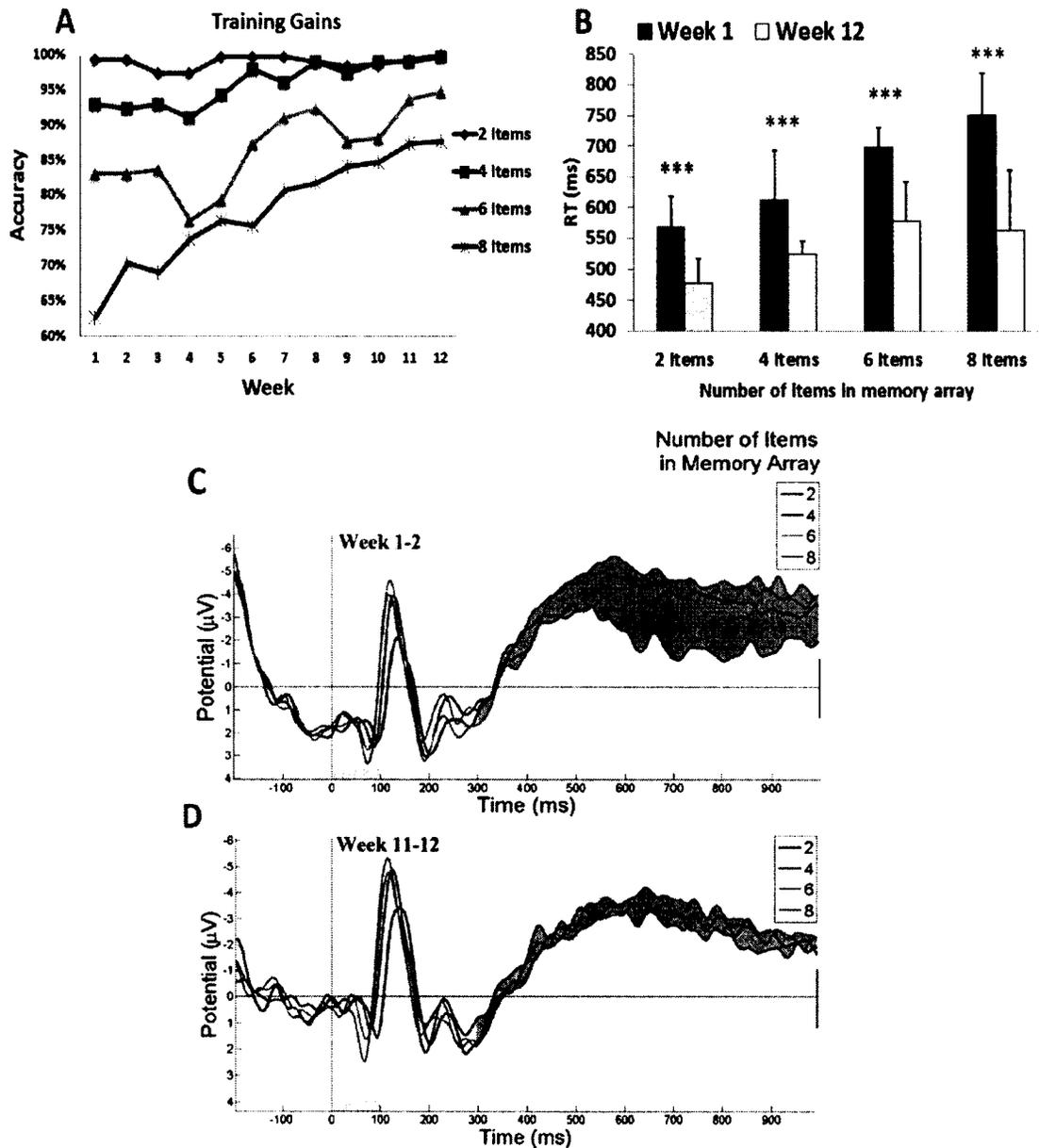
Figure 35: A. VWM training gains within the 12-week intervention period. The overall VWM performance was improved week by week. B. The comparison of RT results between the first and the last weeks. The 12th week was faster than the first week in all conditions. C-D. ERP waveforms using the same conventions defined in Figure 3A are shown. The average N1 amplitude (100 - 180 ms) and the CDA amplitude for the 2-item trials were significantly lower than the 4-, 6-, and 8-item trials during the first two weeks. However, with weekly training, the averaged CDA changed gradually. Later, the typical amplitude pattern in gray shade (2-item < 4-, 6-, and 8-item) became indistinguishable. Error bars represent confidence intervals. *** p < 0.005.

4.2.3   VWM Transfer Benefit Experiment

The goal of the VWM transfer benefit experiment was to study the impact of training gains on high-level cognitive VWM tasks. Subjects were separated into two groups, training and control groups, to evaluate the behavior evidence and neural activity. Their performance on non-trained tasks was compared between pre-training (TB1) and post-training (TB2) sessions. The neural activity of functional plasticity (TB2 – TB1) that refers to changes of N1 amplitude and CDA can be used as a signal marker to predict VWM accuracy improvement.

The average accuracy improvement of the training group was significantly higher than the control group in 4-item, 6-item, and 8-item (7% vs 3.33%, 7.33% vs 4%, and 8% vs 3.33%, respectively; $p < 0.005$). However, no difference for 2-items (0.67% vs 0%) was found (Figure 36A). In the RT analysis (Figure 36B), the training group's response was faster than the control group in all of the experimental conditions, including TB1 pre-training (584 ms vs. 816 ms; $p < 0.005$; 649 ms vs. 772 ms; $p < 0.005$; 672 ms vs. 796 ms; $p < 0.005$; and 713 ms vs. 752 ms; $p > 0.05$, respectively) and TB2 post-training (517 ms vs. 752 ms; $p < 0.005$; 633 ms vs. 689 ms; $p < 0.05$; 723 ms vs. 757 ms; $p > 0.05$ and 780 ms vs. 874 ms; $p < 0.05$, respectively). The result suggests that the trainees felt more confident performing tasks than the controls.

The ERP analysis of the VWM transfer benefit was focused on N1 amplitude and CDA in the 8-item condition, because the more difficult task showed the greatest improvement (TB2 – TB1: 8%) for the trainees. For the training group, N1 amplitude and CDA were significantly different at TB1 and TB2 as shown in Figure 36C (N1: -3.67 μV vs. -2.43 μV; $p < 0.05$; CDA: -2.91 μV vs. -1.52 μV; $p < 0.005$). However, there was no

significant difference in N1 and CDA for the control group in Figure 36D (N1: -3.50 μV vs. -3.06 μV; p = 0.42; CDA: -2.75 μV vs. -2.64 μV; p = 0.09). This diminished N1 and CDA could be used as a predictor of VWM training gains on non-trained tasks. This was also consistent with this study's hypothesis for the VWM load experiment where CDA changes in ERP stimuli would lead to improved memory capacity and VWM performance. Recent reports have implicated that training can enhance VWM capacity and attention over time and can increase the brain activity in the prefrontal and parietal cortex [33]. We analyzed the transfer benefits by proposing a subtractive measure in which the difference between the post-training TB2 and the pre-training TB1 was computed for both training and control groups. The positive increase in neural activity was consistent with the notion of neuroplasticity generated by training [31]. For the control group, no significant change in ERP activity was observed. These cognitive improvement findings are important for demonstrating the strength of the adaptive training gains on non-trained tasks by providing behavior evidence and neural mechanism.
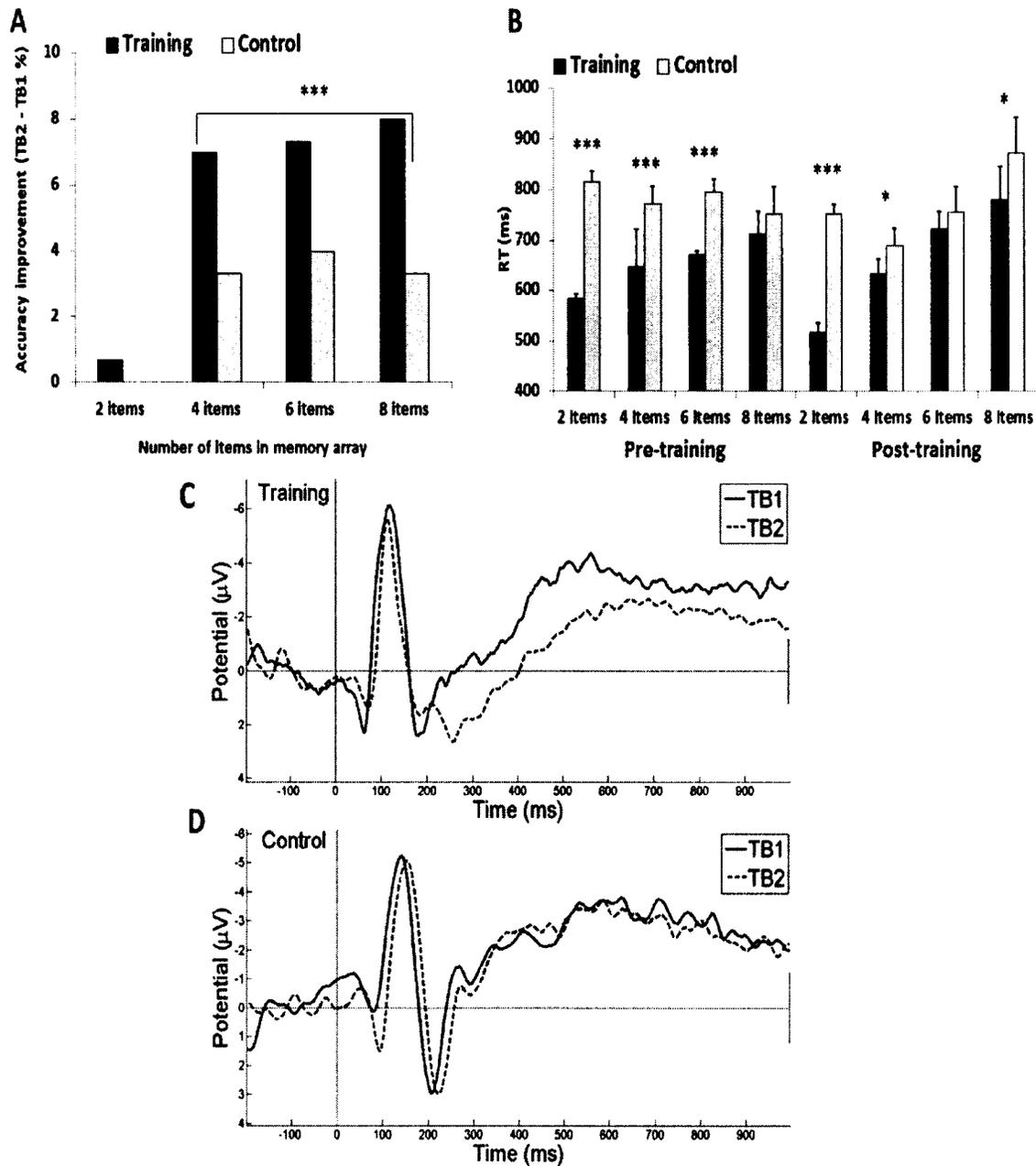
Figure 36: A. VWM transfer benefits experiment between subjects with and without weekly training. The training group achieved a significant improvement over the control group. B. Comparison of RT results between training and control groups for pre-training and post-training sessions. C-D. Grand average ERPs are shown. The N1 amplitude (90 - 170 ms after cue) and the CDA have significantly diminished for the training group at TB2 (NI: -3.67 μV vs. -2.43 μV; p < 0.05; CDA: -2.91μV vs. -1.52 μV, respectively; p < 0.005), but not for the control group (NI: -3.50μV vs. -3.06 μV; p = 0.42; CDA: -2.75 μV vs. -2.64 μV, respectively; p = 0.09). Error bars represent confidence intervals. * p < 0.05, *** p < 0.005.

CHAPTER 5

DISCUSSION

5.1   Decoding Motor Intention through EEG BCI

BCI technology enables people to interact with external devices in new and intuitive ways. As a prosthetic application, it helps people with limited muscle control (such as those suffering from spinal injury, stroke or cerebral palsy) regain some of the lost motor functions. Even though there is still debate over the best classification method for BCI, we developed and validated the use of surface EEG to distinguish the brain activity during planning of intended arm movements. EEG data was recorded from untrained subjects excluding feedback, where each individual subject was analyzed independently in this study. Subjects only instructed to perform the indicated reaching tasks (see Figure 3). In the framework of upper limb neuroprosthesis, this paradigm could be directly implemented as a part of the control strategy of the prosthetic arm for activity of daily living (ADL).

The spatial, temporal, and spectral features were extracted based on reported literature. We used the spatial information near the PPC regions as previously reported [16]. The temporal feature pertaining to the mean EEG signal amplitude 271-310 ms, after the presentation of the "Direction cue", the visual-cue was found to have the most significant difference between the intended arm reaching directions, and the highest

57

classification accuracy. A scaling strategy based on the EEG response to cue-based stimulus was proposed. The maxima and minima "signature" signal from 0–235 ms after the presentation of the "Direction cue" was used as a scaling factor for subsequent single-trial analysis. The early synchronization in the delta (0-4 Hz) and low theta (4-8 Hz) bands is related to the "Direction cue", which supports the idea of early component reflects the processing of the visual intention, where the alpha band (9-12 Hz) is associated with the visual attention [83]. The "signature" signal around this frequency range can be found at different recording electrodes near the ROIs and the visual cortex during the delayed "Direction cue" period. The utility of the proposed cue-based "signature" scaling factor gave some promising results by improving the classification accuracy of intended motor directions. To test this scaling strategy in more realistic situations, it may be extended to non-visual cue based (voluntary movement) setup. In these experiments, the subjects will decide the desired reaching destinations without the target-specific stimulation. The "signatures" in these situations would have been internally triggered, possibly dominated by a slightly different frequency component.

Our current study did not attempt to distinguish the three effectors. Recently, there have been many reported studies on the classification of saccade motor imagery versus motor execution tasks [22, 84, 85]. In the future, a combination of motor planning and motor imagery for amputee subjects may be a more viable technique for controlling neuroprosthetics devices. Another future improvement includes the use of non-invasive mobile prosthetic platform via wireless dry electrodes and wearable EEG systems would benefit in real world operational environments [86, 87]. Before the implementation of a real-time BCI system, some hardware platforms and specific software need to be

developed. Future development of specific software communication systems between EEG recording devices and signal processing platform must be designed and operated close to real-time. Other specification includes simple training protocol for rehabilitation purposes. More work is needed to understand how changes in attention and intention may impact EEG signals. Future study related to the angular direction decoding, instead of the current discrete directions, may be necessary. Participants with motor-disabilities will be recruited to provide more conclusive results on the advantage of the proposed "signature" scaling and classification algorithms.

5.2   Monitoring Visual Working Memory Though EEG BCI

The second part of this study demonstrates the long-term effects of VWM load, training gains and transfer benefits. In summary, we found that (1) the VWM capacity can be estimated based on accuracy and CDA level. These are also highly related to reaction time, VWM capacity, and CDA. Neural evidence for VWM capacity limit, which approximates the "magic number 4" [75], is observed in ERP waveforms. The average capacity across 15 participants is 2.8 items, which is similar to Emrich's result [88]. (2) VWM capacity can be improved through adaptive training over a long period of time. We are particularly interested in a longer training period (up to 12 weeks) than other previous studies (5 weeks) [89]. The reaction time improved after 12-weeks of training in all 2-item, 4-item, 6-item, and 8-item conditions, which suggests that the participants may have felt more confident performing tasks in the last week than the first week. (3) Trainees have higher accuracy improvement than the control group. The increased activity in the posterior partial cortex was obtained in a subtractive measure (TB2 – TB1) which was the difference between post-training and pre-training

performance for trainees. The diminished N1 and CDA can be used as a neural marker of VWM training gains on non-trained tasks where CDA changes in ERP stimuli led to improved memory capacity and VWM performance. The improvement measurement also relates to the strength of the adaptive training gains on non-trained tasks by providing behavior evidence and neural mechanism. Overall, these results support our hypothesis that all participants can benefit from training gains, and demonstrate the sustained impacts on VWM capacity over a long period of time. Moreover, this training method may be useful for enhancing cognitive function through training.

VWM plays a critical role in change-detection, especially when the memory array becomes more complex. VWM becomes more demanding as the memory array becomes more difficult [27]. Low-item conditions results in less information, more efficient, higher accuracy, and low CDA amplitude. On the other hand, when many items are in a memory array, the subjects' recall complex information is less efficient, resulting in lower accuracy and higher CDA amplitude. Furthermore, individuals with low memory capacity depend on more working memory to perform VWM tasks. In contrast, participants with high memory capacity could perform VWM tasks much more easily and efficiently. Likewise, they are able to process and store more information during the VWM experiments. This arrangement was supported by the correlation to accuracy, reaction time, VWM capacity, and CDA in VWM load experiments (Figures 32-34), representing that high-capacity individuals were more accurate and efficient in more complex conditions than low-capacity individuals.

The results of this study demonstrate that CDA component can be used to predict the individual's VWM capacity. The CDA pattern in ERP waveform (Figure 35C) was

similar to others' findings in which the CDA amplitude from 2-object searching was twice as high as for a single target [73]. Meanwhile, the CDA disappeared when the subjects were repeating the same searching tasks after a short period of time [90], which is consistent with our outcomes from training gain experiments in Figure 35C-D. This situation can be explained considering that the subjects had to pay more attention in the early training period (weeks 1-2). However, with regular training, the CDA changed gradually over time, resulting in a negligible difference between the CDA patterns in these conditions (weeks 11-12). This might be due to the fact that the participants' VWM capacities were enhanced by training, or changed by the transition from a short-term memory to a long-term memory.

The present study also focuses on the differences between trainees and controls in the transfer benefit experiment. Training gains and transfer effects were maintained across the 12-week intervention period. The subtractive measure in transfer benefits displays that plasticity induced by training often appears in VWM and attention [91]. This study may help with cognitive decline due to normal aging and memory deficits can be overcome by training and medication [92]. The comparison between young and old adults would help in understanding the training gains and transfer effects in the system's development [93-95], though we can expect that there are significant training gains for young adults in most of VWM training paradigms.

One possibility is that this study can be considered as a diagnostic tool for the early stage screening of age-related disease, such as mild cognitive impairment (MCI) and Alzheimer's disease (AD) [96]. VWM coupled with quantified EEG has been used to distinguish mild dementia from normal aging controls [97]. Working memory tasks have

also been applied to study schizophrenia patients [30] where prefrontal inefficiency and cognitive deficits were found. Recent studies have suggested that new neurons are generated by the brain throughout their entire lifespan, so adaptive training and cognitive exercises may have a positive impact on building up strong neural connections and creating new brain networks [33, 98]. Overall, VWM tasks combined with EEG measurments will have the potential to serve as a diagnostic tool in the clinical environment and provide insights into the activity of cognitive behavior.

Our method may be extended on a useful tool to predict age-related trends in memory capacity through machine learning technique [96]. We are also interested in investigating how practice and training impact an individual's performance as one ages [99], and the efficiencies of different training programs for different age groups. The research in VWM raises many unanswered questions, such as the optimal duration period and the amount of training time. Likewise, the comparison between visual WM and verbal WM tests will be necessary to improve the working memory method development. Brain computer interface (BCI) technology allows direct communication to occur between the brain and an external machine [1], and its application can range from medical devices to entertainment [100]. A wearable and wireless brain computer interface device with novel dry electrodes can be applied to this VWM study [101, 102]. We believe that the plasticity of the brain enables it to become more effective in memory, attention, processing information, thinking innovation, and solving problems [103, 104] through effective novel brain training simulations [105]. An advanced monitoring system with both wireless BCI and effectual simulations which provides neural activity and

behavior evidence in real-time will be popular and easy to operate for people who seek to enhance their academic ability and daily performance.

This experimental approach is sensitive and accurate, since the device can directly detect the neural activity changes from posterior parietal electrodes contralateral to the location of the cue in each trial [44, 106]. Likewise, compared to other neuroimaging methods [45, 46], such as functional magnetic resonance image (fMRI), EEG is low cost, less time consuming and easier to operate. It is simple to modify our EEG-based visual tasks to other paradigms to study VWM. Another important difference between EEG and fMRI is that EEG is able to resolve hemodynamic changes of integrated cognitive activity over milliseconds, while the fMRI only requires the resolution over a few seconds [47]. This helps to understand the short term memory representation, and predict one's cognitive ability through VWM tasks. Specifically, CDA is considered as an indicator of an individual's memory capacity.

The future aims are to expand my research in (1) An advanced monitoring system with both wireless BCI and effectual simulations that provides neural activity and behavior evidence in real-time will be popular and easy to operate for people who seek to enhance their academic ability and daily performance. (2) VWM combined with EEG measurement will have the potential to serve as a diagnostic tool in the clinical environment and provide insights into the activity of cognitive manners. (3) Designing a useful system to predict age-related trends in memory capacity through machine learning technique. (4) Creating a new adaptive training and cognitive exercises to make a positive impact on building up strong neural connections and creating new brain networks. (5)

Brain function relating action and perception is an attractive subject, especially decision-

making. It is so interesting to understand human choice behavior.

CHAPTER 6

CONCLUSIONS

A hybrid BCI approach can be used to control the directions of intended arm movement on neuroprosthetics devices and to monitor for individuals VWM capacity which can benefit from adaptive training. Although surface EEG signals have limit information about complex arm movements, we have demonstrated EEG signal can be used to decode the direction of the reaching tasks during the planning stage prior to the actual motion. Visual cue-based experiments were designed to provide visual-cues to guide the user saccade/arm movements. ICA and EEMD are efficient to remove artifacts. The estimate of source localization related to the motor intention is found at PPC. An amplitude scaling strategy has been developed to adjust the trial-to-trial variability in the EEG signal amplitude near the PPC regions. Temporal information (271-310 ms) after the presentation of the visual cues is found to hold the most discriminatory features. This work would have direct application based on the electrographical signals of the user's intent. In addition, motor intention combined with motor imagery paradigm would provide more commands on the control of BCI. The overall single-trial classification accuracy of 93.91 ± 6.09% holds this paradigm promising for noninvasive BCI design in neuromotor prosthesis or wheelchair applications. The results reveal that VWM capacity is directly correlated to the RT and CDA amplitude. The approximate "magic number 4"

has been observed through the ERPs patterns, where the average capacity is 2.8-item from 15 participants. In addition, VWM capacity can be improved through adaptive training. Furthermore, participants from the training group are able to improve their performance accuracies dramatically compared to the control group. Transfer benefits from adaptive training can also be observed at 12 weeks after training". Therefore, we conclude that all participants can benefit from training gains, and augmented VWM capacity can be sustained over a long period of time. Our results suggest that this form of training can significantly improve cognitive function and may be useful for enhancing the user performance on neuroprosthetics devices. The more we learn about the neural mechanisms linking thoughts, movements and perceptions, the better we can address therapeutic approaches to prolong useful life and cognitive decline. The ultimate research goal is to create marketable systems for individuals' needs and to accelerate translational research.

APPENDIX A

EEG STANDARD OPERATING PROCEDURES

Important Notes:

- Make sure everything is plugged into the white box

- Ensure that the firewire ports are connected to the correct sides

- Check to see if the participants have any allergic reactions (Potassium Chloride (KCl,) Baby shampoo, etc.)

- Ask that Cellphones be turned off (Not silent). Electronic devices might create artifacts on the EEG recording.

- Check and ask participant to remove earrings, piercings, or anything else that might catch on the hair net.

- Ask and check to see that the participant does not have hair gel, hairspray, dreadlocks, corn rows, temporary hair dye, or conditioner.

- Check that the participant is not chewing gum.

Setup:

1) Turn on computer.

> Username: EGI

> Password: Geodesic   (No 's')

2) Open Net Station program.

3) Check that the first two numbers for the version number and HASP (Hardware and Software Protection) match. HASP is located at the bottom left corner of window.

    a.   If an update is needed.

          Click HASP updater.

          Zip the HASP file.

          Send to support.

          Unzip response and drag HASP file back into the HASP updater.

    b.   Move on the next step.

4) Create Acquisition Setup or select previously created Acquisition Setup.

    a.   Open "Workbench".

    b.   Place:

          Net Amp 300

          First Order High Pass

          Digital Filter

          Bipolar Montage (Optional)

          Display TCP/IP (Optional)

          Dense Waveform Display

          Multiport Simulator

          Waveform Recorder

    c.   Configure First Order High Pass to 0.10 then turn on.

    d.   Open panels (windows).

          Make sure the hair net is not hooked up.

          Turn on the program and it will automatically start a "Gains" test.

          If there is an error, run the "Gains" test 2-3 more times.

          If the error continues to appear, conduct the "Bucket" test.

Bucket Test.

Do not conduct on participant's head.

[Need to double check procedure for Bucket Test].

e. When no errors are indicated, then proceed to turn off the workbench.

f. Click on the workbench to close everything.

Session Template:

1) Create Session Template or select Standard Session Template.

2) Click Calibrate Template.

3) Select the appropriate Acquisition setup from the list.

a. Choose Metric fields and insert.

Select Metrics (i.e First Name, Gender, Age, etc.).

Select Subject/Date/Time.

b. Close.

Open up Session:

1) Click Session. The workbench and all panels should open.

2) Enter the name of the session.

Putting on Hair Net:

1) Double check that the participant does not have any of the following:

a. Hair gel, hairspray, dreadlocks, corn rows, temporary dye, conditioner, earrings, piercings, or anything that will catch on the hair net.

b. Check to see if the participant has any allergic reactions to Potassium Chloride (KCl) or baby shampoo.

c. Check that the participant is not chewing gum.

2) Measurements:

    a. Start from the middle of the eyebrow ridge (Nasion) and go around the head. Make sure the measuring tape is above the ear and goes around the Lambda (bump at the back of the skull).

    b. Determine which net to use. If the individual is between sizes, then utilize the smaller net.

    c. Note the size used for the experiment.

3) Prepare hair net:

    a. Fill Electrolyte Bucket with one liter of warm water.

    b. Add one spoonful of KCl and one spoonful of shampoo. Use the appropriate spoons.

    c. Stir with the shampoo spoon.

    d. Place hair net into the solution. Agitate the solution by dunking the hair net four times into the bucket.

    e. Let the hair net sit for five minutes. The hair net can sit in the solution between 5-20 minutes.

    f. Make sure the net is completely underwater.

    g. If necessary, make the Disinfectant Solution now. (See Making Disinfectant Solution).

4) Measure the "Placement Point" for the "Reference" electrode (REF):

    a. Inform the participant that you will be marking the top of the head for a reference point.

b. Start from the Nasion and go over the top of the head to the depression point below the bump (Lambda) at the back of the skull.

c. Mark the top of the head with the red pencil at the half way point.

d. Then measure the head from the open jaw on one side of the head to the other. Ask the participant to open and close mouth. Or measure from ear to ear, if they are leveled.

e. Mark the top of the head with the red pencil at the half way point. Make sure that this mark crosses the previous mark.

5) Explain the experiment while waiting for the hair net to soak up the electrolytes:

a. Check for chewing gum.

b. Explain to the participant to stay as still as possible while the experiment is in progress.

6) Place towels over the shoulders of the participant.

7) Turn on the PC and start up E-Prime.

8) Placement of hair net.

a. Have participant hold the connection end of the hair net.

b. Instruct participant to close eyes.

c. Stick hands into hair net. Thumbs are placed one electrode outside of nose guard and under the double plastic lines. Pinkies should extend to the back near the last row.

d. Place REF electrode on the target marked previously.

e. Stretch out hands and pull Net down over the head.

f. Adjust ears, nose guard and chin straps. Caution: Never pull a single electrode. Pull in clumps.

    i. Tighten chin strap first.

    ii. Adjust the checked electrodes and make sure the wires and straps are not in front of the eyes.

    iii. Hold down the white knob while grabbing the white strand and pull the red strand.

    iv. Then hold down the white knob while grabbing the red strand and pull the white strand.

    v. Then hold down the white knob and both white and red strands and pull down on the chin strap.

    vi. After tightening both sides, retighten the chin strap.

g. Make sure that there is nothing blocking the eyes and check with participant to see if anything is irritating the eyes.

h. Line up the reference points of the Mastoids (Both vertically and Horizontally).

i. Make sure participant is comfortable. Too much blinking will cause artifacts on the EEG. If patient wears glasses, place the glasses over the hair net.

j. Rub in electrodes. Make sure to rub hard enough to shake head in order to ensure skin contact.

k. Have participant open eyes and check visibility.

9) Move participant to the testing chair.

10) Insert the connection end into the arm. Caution: DO NOT FORCE THE CONNECTION INTO THE ARM. Check that knob is 180 degrees from the reference pin. (There are two pins on the connecting end. The reference pin is the pin that is offset from the center.) Then turn the knob to lock the connection.

11) Test for Impedance.

12) Change the monitor switch to MAC.

13) Slide Impedance Chart over to the edge of the screen.

14) Rewet and rub in the electrodes that are indicated in red on the Impedance Chart.

15) Make sure to rewet the REF and COM electrodes (located 2 electrodes down from the REF electrode) even if the Impedance Chart shows all green responses.

16) Close and save Impedance Test.

17) Make sure participant is sitting in a comfortable position that will require little movement to touch the signal pad.

Beginning Experiment:

1) Open E-Prime.

2) Click ok to all of the dialogue boxes.

3) Change the monitor switch to PC.

4) Check to see if participant sees the screen for the test.

5) When ready to begin experiment, click on the "Running Man".

6) On MAC, comments and notes can be made on the EEG recording.

    a. Hold Command (comma) to insert comments.

    b. Click on tabs for eyeblink, eye movement, etc.

7) When done click close session button.

Removing hair net:

1) Unhook the connection end of the hair net.

2) Have participant hold onto the connection end.

3) Instruct the participant to close eyes.

4) Loosen the chin strap and pull all three white knobs all the way down.

5) Stick thumbs under the chin strap and push up underneath the hair net up to the eyebrows.

6) Use the outer fingers to peel the net away from the head.

7) Empty the Electrolyte Bucket into the sink.

8) Rinse the hair net four times with water. Dunk the net into the Electrolyte Bucket until about ¾ full.

9) Place the hair net into the Disinfectant Bucket. Dunk a few times and let sit for ten minutes.

10) Rinse the hair net four times under the water. Dunk the net into the Electrolyte Bucket until about ¾ full.

11) Store Net away on the hair net hooks behind the door.

Making Disinfectant Solution:

1) Fill the Disinfectant Bucket with two liters of distilled water.

2) Add one scoop of disinfectant.

3) The disinfectant lasts for 2 weeks. Mark the expiration date on the bucket. After the expiration, utilize a test strip to see if the disinfectant is still useable.

4) If it is good, then you can use the disinfectant for another week. Mark new date on the bucket.

5) If the disinfectant is no longer good, then dispose of the disinfectant.

Processing Data:

1) Select the Waveform Tool.

2) Create tool or select a previously created tool.

3) If creating a tool, then use a consistent naming convention. (i.e. Person's initial then 2 digit number).

4) Select First Order High Pass. Name 01.

5) Select Filtering. Name 02. Set 30 hz Low-pass.

6) Select Segmentation. Name 03.

7) Select Artifact Detection. Name 04.

8) Create script named Preprocessing. Highlight and drag 01-04.

9) Select Bad Channel Replacement. Name 06.

10) Select Averaging. Name 07.

11) Select Montage Operations. Name 08.

   Select Hydrocell GSN 128.1.0.

   Select Average Reference.

12) Select Baseline Correction. Name 09.

   Baseline set to 100 ms before and 100 ms long.

13) Create script named Postprocessing. Highlight and drag 06-09.

   Use data from Preprocessing. This should be the last one on the dialog box.

APPENDIX B

TOOLS

B.1   E-Prime 2 Stimulation Program Protocol

E-Prime is a graphical interface software applications suite conducting psychological and neuroscientific approaches. It offers control over almost every aspect of paradigm creation, and is temporally accurate to within a few milliseconds, a crucial aspect of control for many research needs. E-Prime takes you through the creation of your experiment to performing descriptive statistics on your collected data.

The E-Prime suite of functions offers the user control over every part characteristic to data analysis in a research application. The core system comprises: E-Studio, E-Basic, E-Run, E-Merge, E-DataAid, and E-Recovery (Figure 37).
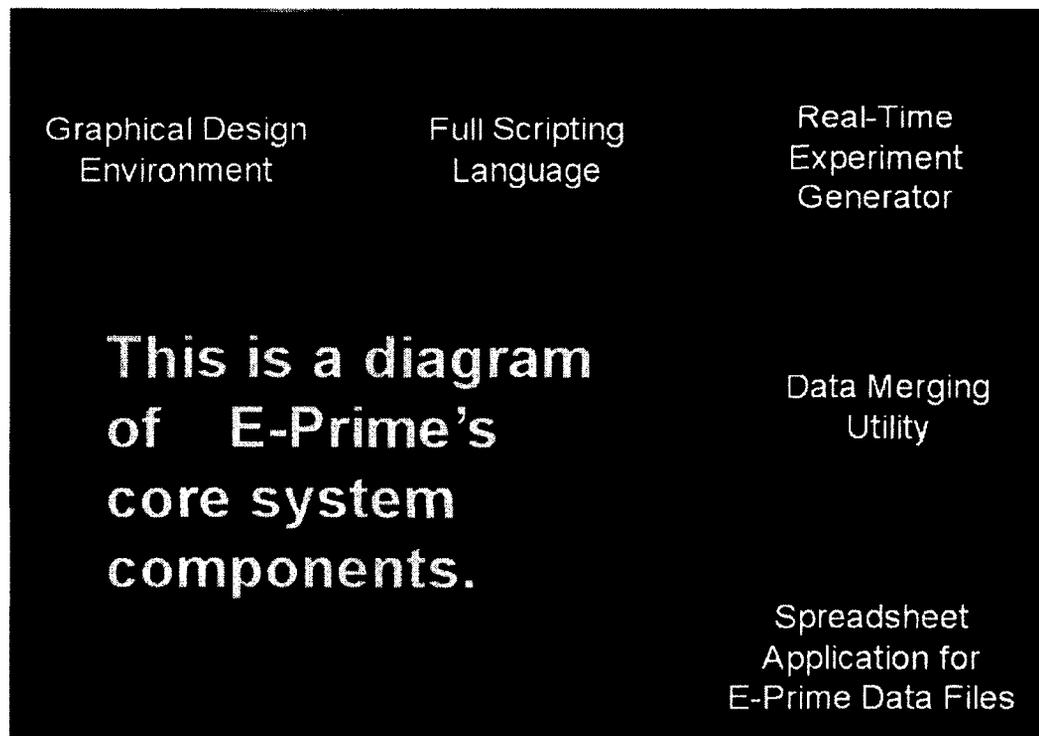
Figure 37: E-prime 2.0 core system components.

E-Studio: E-Studio's graphical environment greatly speeds up the creation of an experiment. Better yet, you can implement most experiment designs without the use of code.

E-Basic: It is E-Prime's comprehensive, object-oriented programming language. It is similar to Visual Basic for Applications with many enhanced commands for behavioral research.

E-Run: E-Run is E-Prime's real-time experiment generator. It compiles E-Basic code from the experiment that you visually created in E-Studio and executes it in a real-time environment.

E-Merge: Merge the individual data files into one file using E-Merge. View, edit, and analyze individual or merged data files in E-DataAid.

E-DataAid: E-DataAid allows you to view and edit your E-Prime data.

E-Recovery: Users can use this program to recover some of the information that was gathered already.

B.2   Waveform Tools

In filtering, filter out activity in frequencies that are not of interest. Normally, the brain activity has been focused on frequencies below 30 or 40 Hz. Note that if you do a low-pass filter in this range, then the 50 Hz or 60 Hz line noise will be filtered out, so there is no need to apply a notch filter. In the experiment, all trials have a band-pass filtered range of 0.1-30 HZ (Figure 38).
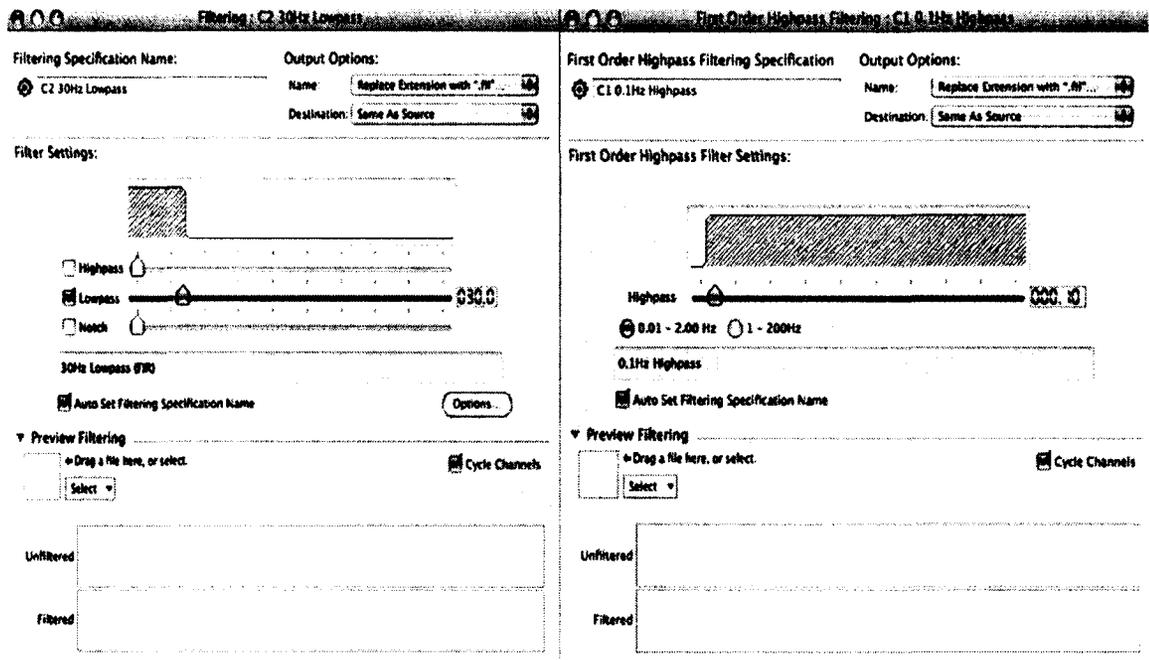
Figure 38: Illustration of low-pass and high-pass filters setup.

In segmentation, it reduces your data to segments (short epochs) that fall into different categories or retention interval. Define the criteria for the categories. Each category is temporally referenced to an event of interest, for a specific experimental condition of interest. You specify the duration, before and after the reference event, to include in the segment. Here, we first broke down the trials for each subject into five directions (right, left, center, up, down). In each direction included the three effectors. Length is 0 to 700 ms following direction cue onset that labeled by movement direction "dir+" (Figure 39).
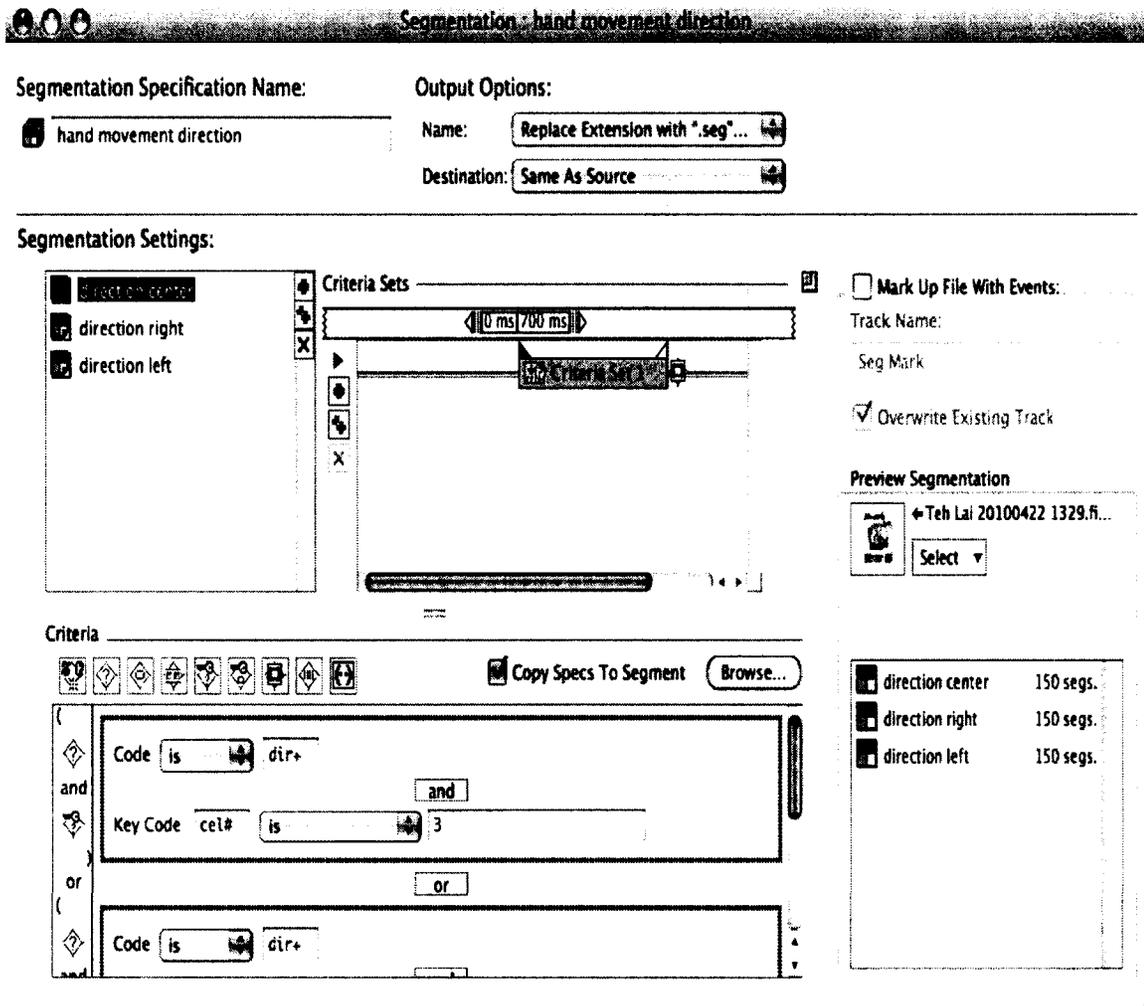
Figure 39: Illustration of segmentation setup for our intended arm movement study.

In artifact detection (Figure 40), automatically detect and mark bad channels and bad segments (which are segments that are contaminated by artifacts). In Figure 41 below, you can see how many segments each channel is bad. Electrodes with poor skin conductively are identified by abnormal activity patterns and removed from the EEG signal data.
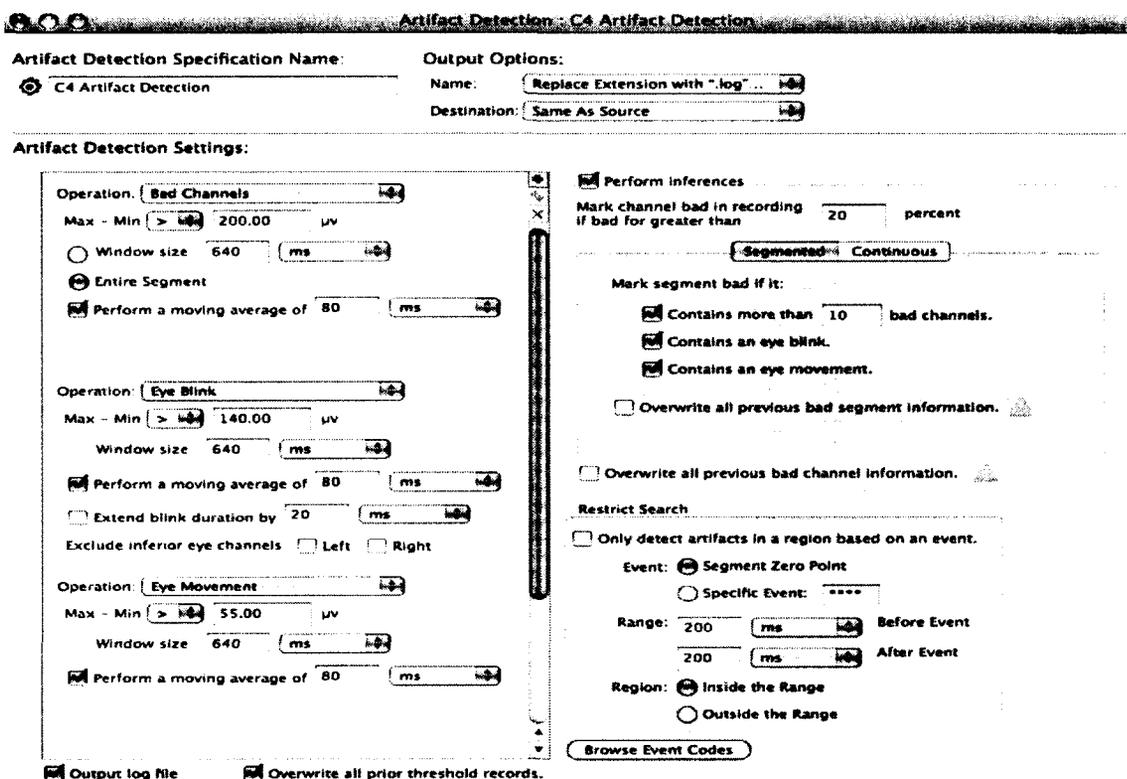
Figure 40: Illustration of artifact detection.

Figure 41: Number of good segments/ total number of segments.

In bad channel replacement (Figure 42), we replace the data in the bad channels with data interpolated from the remaining channels. Bad channel replacement is based on the idea that because of electrical volume conduction, channels in proximity to each other

will have similar data. This approximation increases in validity as the channel count increases. For 128 channels, the results of bad channel replacement are quite good, but for channel counts less than 64, considerable and serious errors exist in the reconstructed data.
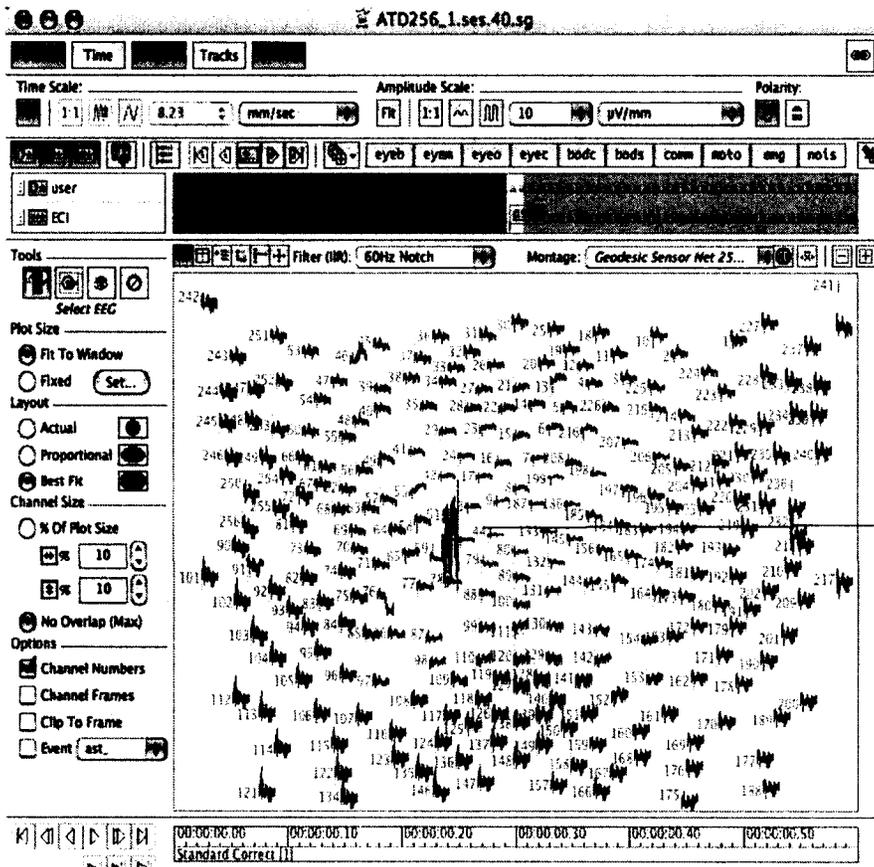
Figure 42: Data in Topo Plot view before bad channel correction.

In averaging, we calculate a single, average segment from all the segments that are not rejected.

In baseline correction, we establish a baseline interval within our segment. We select the interval to use as the baseline. For the experiment, baseline is the period of direction cue onset from -200 to 0 ms before onset for each trial.

B.3   Ensemble Empirical Mode Decomposition

Ensemble empirical mode decomposition (EEMD) is a data-driven analysis method that separates the signal into a collection of intrinsic mode functions (IMFs). It is a powerful approach for analyzing nonlinear, non-stationary EEG signal since the method is only based on local characteristic time scale [55-57]. Unlike other bandpass filters, phase shifts were not introduced using EEMD. It breaks down the signals in a subject dependent manner, which is strictly based on the signal characteristics without specifying any frequency bands [64]. Empirical mode decomposition (EMD) has mode mixing problem where EEMD can solve it by utilizing the uniformly distributed reference frame using the addition of white noise [65]. The procedure for EEMD is described in [56] is summarized below:

S1: Add a white noise $\eta_j(t)$ to the EEG data $x(t)$ to give $x_j(t)$. The standard deviation of $\eta_j(t)$ is 10% of the standard deviation of $x(t)$.

S2: Decompose $x_j(t)$ into IMFs to obtain n-IMFs.

S2.1: Identify all the local extrema in $x_j(t)$, including maxima and minima;

S2.2: Connect all the local maxima and local minima by a cubic spline to create the upper/lower envelope.

S2.3: Calculate a local mean, $m_1(t)$ by averaging the upper and lower envelopes. The difference between $x_j(t)$ and m_1 is the first component $h_1(t)$, i.e.

$$h_1(t) = x_j(t) - m_1(t)$$

S2.4: If $h_1(t)$ is not an IMF, treat $h_1(t)$ as the original signal and repeat S2.1 to

S2.3 until $h_1(t)$ is an IMF.

S2.5: Set $c_1(t) = h_1(t)$ as the first IMF

S2.6: Remove the first component from the original signal and obtain the residue

signal $r_1(t) = x_j(t) - c_1(t)$.

S2.7: Replace $x_j(t)$ in S1 by $r_1(t)$ and repeat S2.1 to S2.6 to obtain other IMFs

until $r_n(t) = r_{n-1}(t) - c_{n-1}(t)$ becomes a monotonic function or a constant.

S3: Repeat S1 and S2 with different white noise series 50 times;

S4: Obtain the ensemble means of the corresponding IMFs. Each IMF can be

considered as a filtered version of the original signal [57].

$$x(t) = \sum_{i=1}^{n} c_i(t) + r_n(t)$$

Eq. 2

We translated a decomposition of the signal into n-IMFs and a residue $r_n(t)$. Each

IMF was then considered as a filtered signal itself [57] from IMF1 to IMF7 (highest to

lowest frequency components). The mathematical equations for obtaining the IMF

analytic signal are given as:

$$z_i(t) = c_i(t) + j\hat{c}_i(t) = a_i(t)e^{j\theta_i(t)}$$

Eq. 3

$$\hat{c}_i(t) = \frac{1}{\pi} p \int_{-\infty}^{\infty} \frac{c_i(\tau)}{t - \tau} d\tau ,$$

Eq. 4

$$a_i(t) = \sqrt{c_i^2(t) + \hat{c}_i^2(t)} ,$$

Eq. 5

$$\theta_i(t) = \arctan \frac{\hat{c}_i(t)}{c_i(t)} .$$

Eq. 6

An illustrative example of the IMFs of an averaged EEG signal and their corresponding power spectra are shown in Figures 43-44.
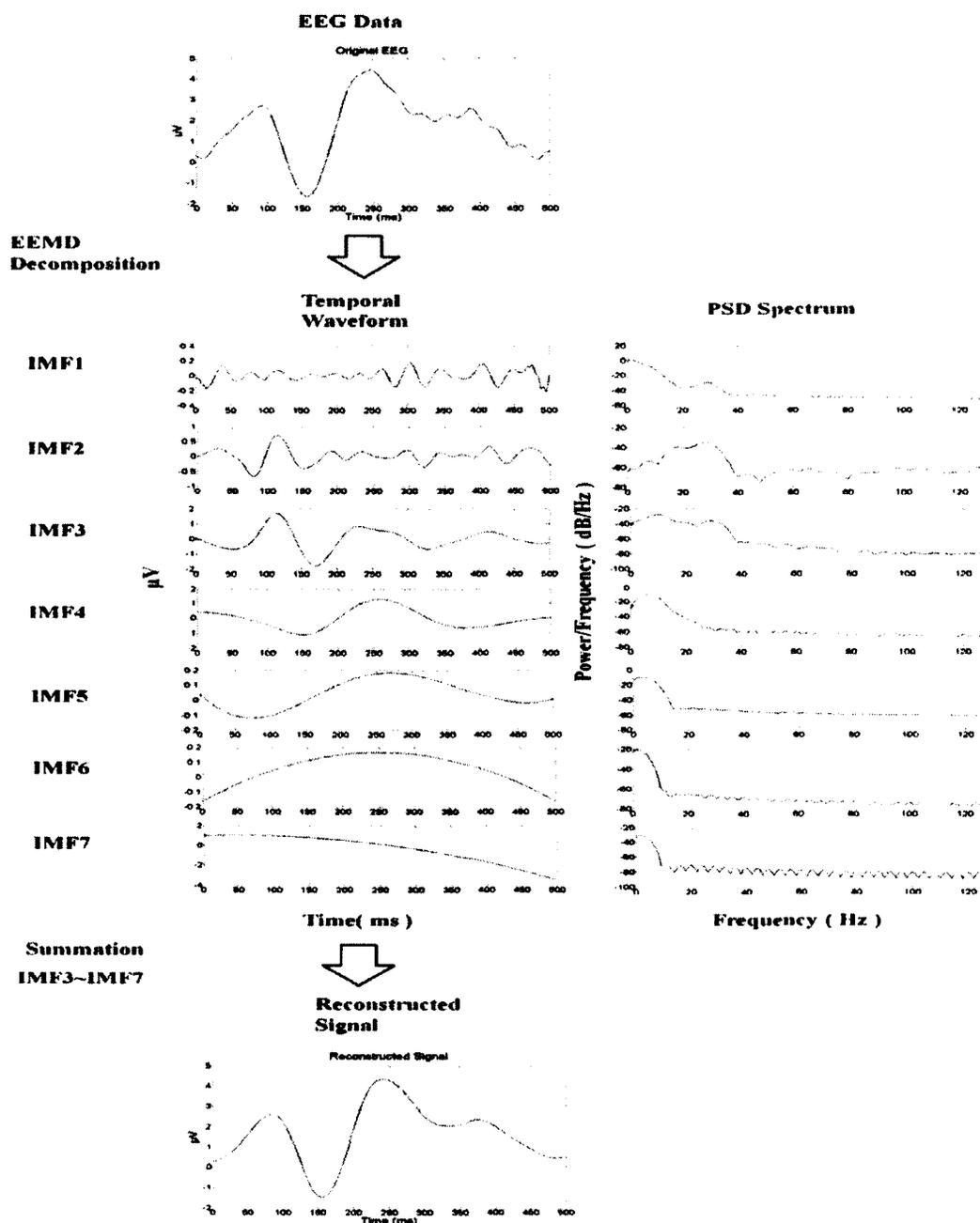
Figure 43: The EEMD decomposition and signal reconstruction procedure. The procedure for computing the IMFs using EEMD is outlined on the left. After collecting the IMFs, the characteristics representing 0.1-30 Hz frequency components were identified using the power spectral density of each mode [25]. High frequency noise can be reduced without phase shifts by removing the low IMFs from the signal reconstruction.
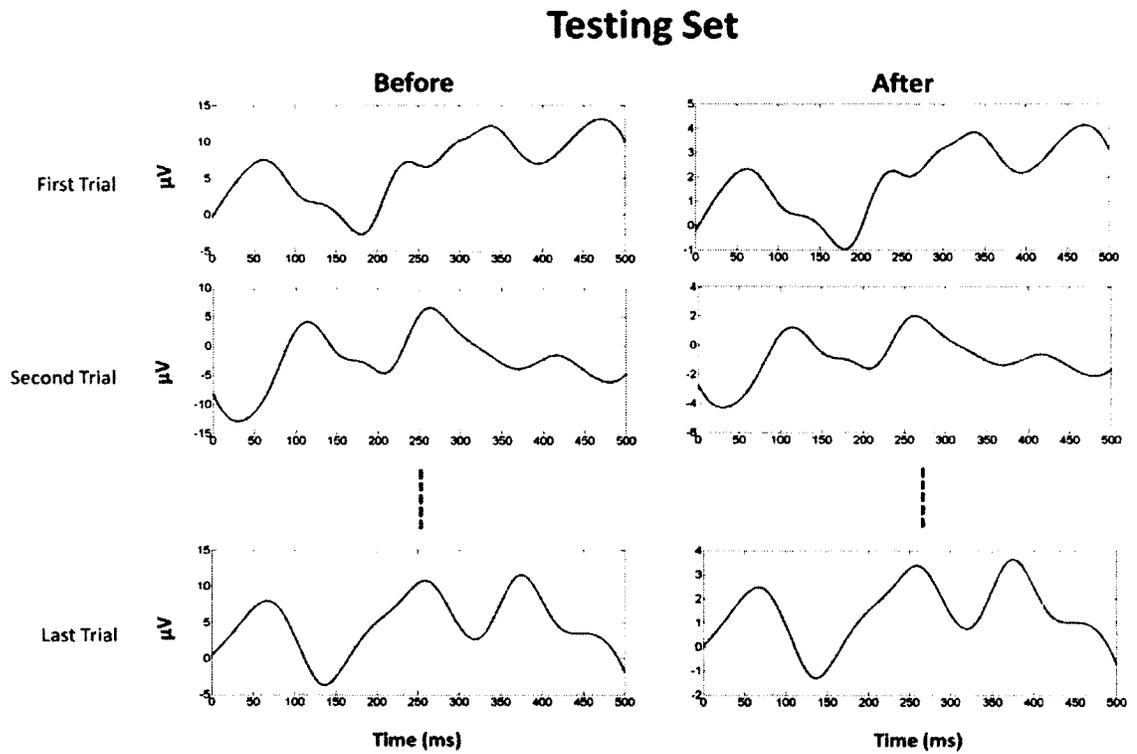
Figure 44: These figures show the difference before and after apply this normalized factor to individual single-trials.

APPENDIX C

IRB APPROVAL LETTER

LOUISIANA TECH
U N I V E R S I T Y

MEMORANDUM

OFFICE OF UNIVERSITY RESEARCH

TO: Dr. Alan Chiu

FROM: Barbara Talbot, University Research

SUBJECT: HUMAN USE COMMITTEE REVIEW

DATE: May 10, 2010

In order to facilitate your project, an EXPEDITED REVIEW has been done for your proposed study entitled:

**"Determining the EG Signals from the Posterior Parietal Cortex to
Decode the Directional Movement of the Arm"**

 # HUC-768

The proposed study's revised procedures were found to provide reasonable and adequate safeguards against possible risks involving human subjects. The information to be collected may be personal in nature or implication. Therefore, diligent care needs to be taken to protect the privacy of the participants and to assure that the data are kept confidential. Informed consent is a critical part of the research process. The subjects must be informed that their participation is voluntary. It is important that consent materials be presented in a language understandable to every participant. If you have participants in your study whose first language is not English, be sure that informed consent materials are adequately explained or translated. Since your reviewed project appears to do no damage to the participants, the Human Use Committee grants approval of the involvement of human subjects as outlined.

Projects should be renewed annually. *This approval was finalized on May 10, 2010 and this project will need to receive a continuation review by the IRB if the project, including data analysis, continues beyond May 10, 2011.* Any discrepancies in procedure or changes that have been made including approved changes should be noted in the review application. Projects involving NIH funds require annual education training to be documented. For more information regarding this, contact the Office of University Research.

You are requested to maintain written records of your procedures, data collected, and subjects involved. These records will need to be available upon request during the conduct of the study and retained by the university for three years after the conclusion of the study. If changes occur in recruiting of subjects, informed consent process or in your research protocol, or if unanticipated problems should arise it is the Researchers responsibility to notify the Office of Research or IRB in writing. The project should be discontinued until modifications can be reviewed and approved.

If you have any questions, please contact Dr. Mary Livingston at 257-4315.

LOUISIANA TECH
U N I V E R S I T Y

OFFICE OF UNIVERSITY RESEARCH   MEMORANDUM

TO: Dr. Alan Chiu

FROM: Barbara Talbot, University Research

SUBJECT: Human Use Committee Review

DATE: August 9, 2012

RE: Approved Continuation of Study HUC 768

TITLE: "Determining the EEG Signals from the Posterior Parietal Cortex to
           Decode the Directional Movement of the Arm"

HUC 768 Renewal

The above referenced study has been approved as of August 9, 2011, 2011 as a continuation of the original study that received approval on May 10, 2010. **This project will need to receive a continuation review by the IRB if the project, including collecting or analyzing data, continues beyond August 9, 2012.** Any discrepancies in procedure or changes that have been made including approved changes should be noted in the review application. Projects involving NIH funds require annual education training to be documented. For more information regarding this, contact the Office of University Research.

You are requested to maintain written records of your procedures, data collected, and subjects involved. These records will need to be available upon request during the conduct of the study and retained by the university for three years after the conclusion of the study. If changes occur in recruiting of subjects, informed consent process or in your research protocol, or if unanticipated problems should arise it is the Researchers responsibility to notify the Office of Research or IRB in writing. The project should be discontinued until modifications can be reviewed and approved.

If you have any questions, please contact Dr. Mary Livingston at 257-4315.

REFERENCE

[1]   J.R. Wolpaw, N. Birbaumer, D.J. McFarland, G. Pfurtscheller, and T.M. Vaughan, "Brain-computer interfaces for communication and control," *Clin Neurophysiol*, vol. 113, (no. 6), pp. 767-91, Jun 2002.

[2]   P.S. Hammon, S. Makeig, H. Poizner, E. Todorov, and V.R.d. Sa, "Predicting Reaching Targets from Human EEG," *IEEE Signal Processing Magazine*, pp. 69-77, Jan 2008.

[3]   A. Nijholt and D. Tan, "Brain-Computer Interfacing for Intelligent Systems," *IEEE Intelligent Systems*, vol. 23, (no. 3), pp. 72-79, 20 May 2008.

[4]   S. Makeig, K. Gramann, T.P. Jung, T.J. Sejnowski, and H. Poizner, "Linking brain, mind and behavior," *Int J Psychophysiol*, vol. 73, (no. 2), pp. 95-100, Aug 2009.

[5]   E.C. Leuthardt, G. Schalk, D. Moran, and J.G. Ojemann, "The emerging world of motor neuroprosthetics: a neurosurgical perspective," *Neurosurgery*, vol. 59, (no. 1), pp. 1-14; discussion 1-14, Jul 2006.

[6]   G. Prasad, P. Herman, D. Coyle, S. McDonough, and J. Crosbie, "Applying a brain-computer interface to support motor imagery practice in people with stroke for upper limb recovery: a feasibility study," *J Neuroeng Rehabil*, vol. 7, pp. 60, 2010.

[7]   A. Bashashati, M. Fatourechi, R.K. Ward, and G.E. Birch, "A survey of signal processing algorithms in brain-computer interfaces based on electrical brain signals," *J Neural Eng*, vol. 4, (no. 2), pp. R32-57, Jun 2007.

[8]   Y.T. Wang, Y. Wang, and T.P. Jung, "A cell-phone-based brain-computer interface for communication in daily life," *J Neural Eng*, vol. 8, (no. 2), pp. 025018, Apr 2011.

[9]   F.C. Sebelius, B.N. Rosen, and G.N. Lundborg, "Refined myoelectric control in below-elbow amputees using artificial neural networks and a data glove," *J Hand Surg Am*, vol. 30, (no. 4), pp. 780-9, Jul 2005.

[10]   J.M. Fontana and A.W.L. Chiu, "Control of Prosthetic Device Using Support Vector Machine Signal Classification Technique," *Am J Biomed Sci*, vol. 1, (no. 4), pp. 336-343, June 2009.

[11]   M. van Gerven, J. Farquhar, R. Schaefer, R. Vlek, J. Geuze, A. Nijholt, N. Ramsey, P. Haselager, L. Vuurpijl, S. Gielen, and P. Desain, "The brain-computer interface cycle," *J Neural Eng*, vol. 6, (no. 4), pp. 041001, Aug 2009.

[12]   T.J. Bradberry, R.J. Gentili, and J.L. Contreras-Vidal, "Reconstructing three-dimensional hand movements from noninvasive electroencephalographic signals," *J Neurosci*, vol. 30, (no. 9), pp. 3432-7, Mar 3 2010.

[13]   Y. Wang and S. Makeig, "Predicting Intended Movement Direction Using EEG from Human Posterior Parietal Cortex," *HCI international conference*, vol. LNAI 5638, pp. 437-446, 2009.

[14]   J.N. Mak, Y. Arbel, J.W. Minett, L.M. McCane, B. Yuksel, D. Ryan, D. Thompson, L. Bianchi, and D. Erdogmus, "Optimizing the P300-based brain-computer interface: current status, limitations and future directions," *J Neural Eng*, vol. 8, (no. 2), pp. 025003, Apr 2011.

[15]   P. Brunner, L. Bianchi, C. Guger, F. Cincotti, and G. Schalk, "Current trends in hardware and software for brain-computer interfaces (BCIs)," *J Neural Eng*, vol. 8, (no. 2), pp. 025001, Apr 2011.

[16]   R. Quian Quiroga, L.H. Snyder, A.P. Batista, H. Cui, and R.A. Andersen, "Movement intention is better predicted than attention in the posterior parietal cortex," *J Neurosci*, vol. 26, (no. 13), pp. 3615-20, Mar 29 2006.

[17]   H.H. Ehrsson, S. Geyer, and E. Naito, "Imagery of voluntary movement of fingers, toes, and tongue activates corresponding body-part-specific motor representations," *J Neurophysiol*, vol. 90, (no. 5), pp. 3304-16, Nov 2003.

[18]   M. Naeem, C. Brunner, R. Leeb, B. Graimann, and G. Pfurtscheller, "Seperability of four-class motor imagery data using independent components analysis," *J Neural Eng*, vol. 3, (no. 3), pp. 208-16, Sep 2006.

[19]   C.F. Pasluosta and A.W.L. Chiu, "Slippage Sensory Feedback and Nonlinear Force Control System for a Low-Cost Prosthetic Hand," *Am J Biomed Sci*, vol. 1, (no. 4), pp. 295-302, June 2009.

[20]   S. Waldert, H. Preissl, E. Demandt, C. Braun, N. Birbaumer, A. Aertsen, and C. Mehring, "Hand movement direction decoded from MEG and EEG," *J Neurosci*, vol. 28, (no. 4), pp. 1000-8, Jan 23 2008.

[21]   S. Waldert, T. Pistohl, C. Braun, T. Ball, A. Aertsen, and C. Mehring, "A review on directional information in neural signals for brain-machine interfaces," *J Physiol Paris*, vol. 103, (no. 3-5), pp. 244-54, Sep-Dec 2009.

[22]   L. Holper and M. Wolf, "Single-trial classification of motor imagery differing in task complexity: a functional near-infrared spectroscopy study," *J Neuroeng Rehabil*, vol. 8, pp. 34, 2011.

[23]   C. Neuper, R. Scherer, S. Wriessnegger, and G. Pfurtscheller, "Motor imagery and action observation: modulation of sensorimotor brain rhythms during mental control of a brain-computer interface," *Clin Neurophysiol*, vol. 120, (no. 2), pp. 239-47, Feb 2009.

[24]   G. Pfurtscheller, R. Leeb, C. Keinrath, D. Friedman, C. Neuper, C. Guger, and M. Slater, "Walking from thought," *Brain Res*, vol. 1071, (no. 1), pp. 145-52, Feb 3 2006.

[25]   Z.X. Zhou, B.K. Wan, D. Ming, and H.Z. Qi, "A novel technique for phase synchrony measurement from the complex motor imaginary potential of combined body and limb action," *J Neural Eng*, vol. 7, (no. 4), pp. 046008, Aug 2010.

[26]   I.R. Olson and Y. Jiang, "Visual short term memory is not improved by training," *Memory & Cognition*, vol. 32, (no. 8), pp. 1326-1332, 2004.

[27]   R. Luria and E.K. Vogel, "Visual search demands dictate reliance on working memory storage," *J Neurosci*, vol. 31, (no. 16), pp. 6199-207, Apr 20 2011.

[28]   Y. Brehmer, H. Westerberg, and L. Backman, "Working-memory training in younger and older adults: training gains, transfer, and maintenance," *Front Hum Neurosci*, vol. 6, pp. 63, 2012.

[29]   A. Jeneson, J.T. Wixted, R.O. Hopkins, and L.R. Squire, "Visual working memory capacity and the medial temporal lobe," *J Neurosci*, vol. 32, (no. 10), pp. 3584-9, Mar 7 2012.

[30]   L. Deserno, P. Sterzer, T. Wustenberg, A. Heinz, and F. Schlagenhauf, "Reduced prefrontal-parietal effective connectivity and working memory deficits in schizophrenia," *J Neurosci*, vol. 32, (no. 1), pp. 12-20, Jan 4 2012.

[31]   A.S. Berry, T.P. Zanto, W.C. Clapp, J.L. Hardy, P.B. Delahunt, H.W. Mahncke, and A. Gazzaley, "The influence of perceptual training on working memory in older adults," *PLoS One*, vol. 5, (no. 7), pp. e11537, 2010.

[32]   J.M. Gold, C.M. Wilk, R.P. McMahon, R.W. Buchanan, and S.J. Luck, "Working memory for visual features and conjunctions in schizophrenia," *J Abnorm Psychol*, vol. 112, (no. 1), pp. 61-71, Feb 2003.

[33]   T. Klingberg, "Training and plasticity of working memory," *Trends Cogn Sci*, vol. 14, (no. 7), pp. 317-24, Jul 2010.

[34]   G. Santhanam, S.I. Ryu, B.M. Yu, A. Afshar, and K.V. Shenoy, "A high-performance brain-computer interface," *Nature*, vol. 442, (no. 7099), pp. 195-8, Jul 13 2006.

[35] T.F. Brady, T. Konkle, and G.A. Alvarez, "A review of visual memory capacity: Beyond individual items and toward structured representations," *J Vis*, vol. 11, (no. 5), pp. 4, 2011.

[36] K. Wendel, O. Vaisanen, J. Malmivuo, N.G. Gencer, B. Vanrumste, P. Durka, R. Magjarevic, S. Supek, M.L. Pascu, H. Fontenelle, and R. Grave de Peralta Menendez, "EEG/MEG source imaging: methods, challenges, and open issues," *Comput Intell Neurosci*, pp. 656092, 2009.

[37] E. Siemkowicz and A.J. Hansen, "Brain extracellular ion composition and EEG activity following 10 minutes ischemia in normo- and hyperglycemic rats," *Stroke*, vol. 12, (no. 2), pp. 236-40, Mar-Apr 1981.

[38] C.M. Michel, M.M. Murray, G. Lantz, S. Gonzalez, L. Spinelli, and R. Grave de Peralta, "EEG source imaging," *Clin Neurophysiol*, vol. 115, (no. 10), pp. 2195-222, Oct 2004.

[39] G. Schalk, J. Kubanek, K.J. Miller, N.R. Anderson, E.C. Leuthardt, J.G. Ojemann, D. Limbrick, D. Moran, L.A. Gerhardt, and J.R. Wolpaw, "Decoding two-dimensional movement trajectories using electrocorticographic signals in humans," *J Neural Eng*, vol. 4, (no. 3), pp. 264-75, Sep 2007.

[40] W. Klimesch, "EEG alpha and theta oscillations reflect cognitive and memory performance: a review and analysis," *Brain Res Brain Res Rev*, vol. 29, (no. 2-3), pp. 169-95, Apr 1999.

[41] T.J. Carew, *Behavioral Neurobiology: The Cellular Organization Of Natural Behavior*: Sinauer Associates, 2000.

[42] B.J. Shannon and R.L. Buckner, "Functional-anatomic correlates of memory retrieval that suggest nontraditional processing roles for multiple distinct regions within posterior parietal cortex," *J Neurosci*, vol. 24, (no. 45), pp. 10084-92, Nov 10 2004.

[43] N. Burgess, K. Jeffery, and J. O'Keefe, *The Hippocampal and Parietal Foundations of Spatial Cognition*: Oxford University Press, 1999.

[44] M. Barinaga, "New imaging methods provide a better view into the brain," *Science*, vol. 276, (no. 5321), pp. 1974-6, Jun 27 1997.

[45] E. Dahlin, A.S. Neely, A. Larsson, L. Backman, and L. Nyberg, "Transfer of learning after updating training mediated by the striatum," *Science*, vol. 320, (no. 5882), pp. 1510-2, Jun 13 2008.

[46] C.D. Moore, M.X. Cohen, and C. Ranganath, "Neural mechanisms of expert skills in visual working memory," *J Neurosci*, vol. 26, (no. 43), pp. 11187-96, Oct 25 2006.

[47]   D.J. Mitchell and R. Cusack, "The temporal evolution of electromagnetic markers sensitive to the capacity limits of visual short-term memory," *Front Hum Neurosci*, vol. 5, pp. 18, 2011.

[48]   F. Darvas, R. Scherer, J.G. Ojemann, R.P. Rao, K.J. Miller, and L.B. Sorensen, "High gamma mapping using EEG," *Neuroimage*, vol. 49, (no. 1), pp. 930-8, Jan 1 2010.

[49]   D.J. Mehagnoul-Schipper, B.F. van der Kallen, W.N. Colier, M.C. van der Sluijs, L.J. van Erning, H.O. Thijssen, B. Oeseburg, W.H. Hoefnagels, and R.W. Jansen, "Simultaneous measurements of cerebral oxygenation changes during brain activation by near-infrared spectroscopy and functional magnetic resonance imaging in healthy young and elderly subjects," *Hum Brain Mapp*, vol. 16, (no. 1), pp. 14-23, May 2002.

[50]   L. Holper, T. Muehlemann, F. Scholkmann, K. Eng, D. Kiper, and M. Wolf, "Testing the potential of a virtual reality neurorehabilitation system during performance of observation, imagery and imitation of motor actions recorded by wireless functional near-infrared spectroscopy (fNIRS)," *J Neuroeng Rehabil*, vol. 7, pp. 57, 2010.

[51]   E.C. Leuthardt, G. Schalk, J.R. Wolpaw, J.G. Ojemann, and D.W. Moran, "A brain-computer interface using electrocorticographic signals in humans," *J Neural Eng*, vol. 1, (no. 2), pp. 63-71, Jun 2004.

[52]   S. Makeig and J. Onton, "ERP Features and EEG Dynamics: An ICA Perspective," *Oxford Handbook of Event-Related Potential Components*, 2009.

[53]   A. Delorme and S. Makeig, "EEGLAB: an open source toolbox for analysis of single-trial EEG dynamics including independent component analysis," *J Neurosci Methods*, vol. 134, (no. 1), pp. 9-21, Mar 15 2004.

[54]   M. Mollazadeh, V. Aggarwal, A.G. Davidson, A.J. Law, N.V. Thakor, and M.H. Schieber, "Spatiotemporal variation of multiple neurophysiological signals in the primary motor cortex during dexterous reach-to-grasp movements," *J Neurosci*, vol. 31, (no. 43), pp. 15531-43, Oct 26 2011.

[55]   N.E. Huang, Z. Shen, S.R. Long, M.C. Wu, and H.H. Liu, "The empirical model decomposition and the Hilbert spectrum for nonlinear and nonstationary time series analysis," *Proc. R. Soc. Lond. A*, vol. 454, pp. 903-995, 1998.

[56]   Z. Wu and N.E. Huang, "Ensemble empirical mode decomposition: A noise-assisted data analysis method," *Advances in Adaptive Data Analysis*, vol. 1, (no.1), pp. 1-41, 2009.

[57]   C.L. Yeh, H.C. Chang, C.H. Wu, and P.L. Lee, "Extraction of single-trial cortical beta oscillatory activities in EEG signals using empirical mode decomposition," *Biomed Eng Online*, vol. 9, pp. 25, 2010.

[58] K.R. Muller, C.W. Anderson, and G.E. Birch, "Linear and nonlinear methods for brain-computer interfaces," *IEEE Trans Neural Syst Rehabil Eng*, vol. 11, (no. 2), pp. 165-9, Jun 2003.

[59] F. Lotte, M. Congedo, A. Lecuyer, F. Lamarche, and B. Arnaldi, "A review of classification algorithms for EEG-based brain-computer interfaces," *J Neural Eng*, vol. 4, (no. 2), pp. R1-R13, Jun 2007.

[60] T. Cooke, "Two variations on Fisher's linear discriminant for pattern recognition," *IEEE Transactions Pattern Analysis and Machine Intelligence*, vol. 24, (no. 2), pp. 268 - 273, 2002.

[61] T.P. Jung, S. Makeig, T.W. Lee, M.J. McKeown, G.Brown, A.J. Bell, and T.J. Sejnowski, "Independent component analysis of biomedical signals," *Proc. 2nd Int. Workshop on Independent Component Analysis and Signal Separation*, pp. 633-644, 2000.

[62] C.T. Lin, S.A. Chen, T.T. Chiu, H.Z. Lin, and L.W. Ko, "Spatial and temporal EEG dynamics of dual-task driving performance," *J Neuroeng Rehabil*, vol. 8, pp. 11, 2011.

[63] R. Oostenveld and T.F. Oostendorp, "Validating the boundary element method for forward and inverse EEG computations in the presence of a hole in the skull," *Hum Brain Mapp*, vol. 17, (no. 3), pp. 179-92, Nov 2002.

[64] W.Y. Hsu, "EEG-based motor imagery classification using neuro-fuzzy prediction and wavelet fractal features," *J Neurosci Methods*, vol. 189, (no. 2), pp. 295-302, Jun 15 2010.

[65] T.Y. Wu and Y.L. Chung, "Misalignment diagnosis of rotating machinery through vibration analysis via the hybrid EEMD and EMD approach," *Smart Materials and Structures*, vol. 18, (no. 9), pp. 095004, 2009.

[66] V. France and V. Hlavac, "Statistical Pattern Recognition Toolbox for Matlab," 2004.

[67] M. Congedo, F. Lotte, and A. Lecuyer, "Classification of movement intention by spatially filtered electromagnetic inverse solutions," *Phys Med Biol*, vol. 51, (no. 8), pp. 1971-89, Apr 21 2006.

[68] P. Flandrin, G. Rilling, and P. Goncalves, "Empirical Mode Decomposition as a Filter Bank," *IEEE Signal Processing Letters*, vol. 11, (no. 2), pp. 112-114, 2004.

[69] Y. Wang and T.P. Jung, "A collaborative brain-computer interface for improving human performance," *PLoS One*, vol. 6, (no. 5), pp. e20422, 2011.

[70] T.P. Jung, S. Makeig, M. Westerfield, J. Townsend, E. Courchesne, and T.J. Sejnowski, "Removal of eye activity artifacts from visual event-related potentials in normal and clinical subjects," *Clin Neurophysiol*, vol. 111, (no. 10), pp. 1745-58, Oct 2000.

[71] J. Onton, A. Delorme, and S. Makeig, "Frontal midline EEG dynamics during working memory," *Neuroimage*, vol. 27, (no. 2), pp. 341-56, Aug 15 2005.

[72] E.K. Vogel and M.G. Machizawa, "Neural activity predicts individual differences in visual working memory capacity," *Nature*, vol. 428, (no. 6984), pp. 748-51, Apr 15 2004.

[73] N.B. Carlisle, J.T. Arita, D. Pardo, and G.F. Woodman, "Attentional templates in visual working memory," *J Neurosci*, vol. 31, (no. 25), pp. 9315-22, Jun 22 2011.

[74] R.J. Itier and M.J. Taylor, "Effects of repetition and configural changes on the development of face recognition processes," *Dev Sci*, vol. 7, (no. 4), pp. 469-87, Sep 2004.

[75] N. Cowan, "The magical number 4 in short-term memory: a reconsideration of mental storage capacity," *Behav Brain Sci*, vol. 24, (no. 1), pp. 87-114; discussion 114-85, Feb 2001.

[76] R. Tombo, Jr., "Engineering Student Statistics," *Science*, vol. 31, (no. 787), pp. 145, Jan 28 1910.

[77] S.J. Luck and E.K. Vogel, "The capacity of visual working memory for features and conjunctions," *Nature*, vol. 390, (no. 6657), pp. 279-81, Nov 20 1997.

[78] A. Gevins, M.E. Smith, L. McEvoy, and D. Yu, "High-resolution EEG mapping of cortical activation related to working memory: effects of task difficulty, type of processing, and practice," *Cereb Cortex*, vol. 7, (no. 4), pp. 374-85, Jun 1997.

[79] N. Pratt, A. Willoughby, and D. Swick, "Effects of working memory load on visual selective attention: behavioral and electrophysiological evidence," *Front Hum Neurosci*, vol. 5, pp. 57, 2011.

[80] K. Fukuda, E. Awh, and E.K. Vogel, "Discrete capacity limits in visual working memory," *Curr Opin Neurobiol*, vol. 20, (no. 2), pp. 177-82, Apr 2010.

[81] T. Drew, T.S. Horowitz, J.M. Wolfe, and E.K. Vogel, "Delineating the neural signatures of tracking spatial position and working memory during attentive tracking," *J Neurosci*, vol. 31, (no. 2), pp. 659-68, Jan 12 2011.

[82] S.A. Hillyard and L. Anllo-Vento, "Event-related brain potentials in the study of visual selective attention," *Proc Natl Acad Sci U S A*, vol. 95, (no. 3), pp. 781-7, Feb 3 1998.

[83] M.S. Treder, A. Bahramisharif, N.M. Schmidt, M.A. van Gerven, and B. Blankertz, "Brain-computer interfacing using modulations of alpha activity induced by covert shifts of attention," *J Neuroeng Rehabil*, vol. 8, pp. 24, 2011.

[84] K.J. Miller, G. Schalk, E.E. Fetz, M. den Nijs, J.G. Ojemann, and R.P. Rao, "Cortical activity during motor execution, motor imagery, and imagery-based online feedback," *Proc Natl Acad Sci U S A*, vol. 107, (no. 9), pp. 4430-5, Mar 2 2010.

[85] E. Raffin, J. Mattout, K.T. Reilly, and P. Giraux, "Disentangling motor execution from motor imagery with the phantom limb," *Brain*, vol. 135, (no. Pt 2), pp. 582-95, Feb 2012.

[86] C.T. Lin, L.W. Ko, J.C. Chiou, J.R. Duann, R.S. Huang, S.F. Liang, T.W. Chiu, and T.P. Jung, "Noninvasive Neural Prostheses Using Mobile and Wireless EEG," *Proceedings of the IEEE*, vol. 96, (no. 7), pp. 1167-1183, July 2008.

[87] C.T. Lin, L.W. Ko, M.H. Chang, J.R. Duann, J.Y. Chen, T.P. Su, and T.P. Jung, "Review of wireless and wearable electroencephalogram systems and brain-computer interfaces--a mini-review," *Gerontology*, vol. 56, (no. 1), pp. 112-9, 2009.

[88] S.M. Emrich, N. Al-Aidroos, J. Pratt, and S. Ferber, "Visual search elicits the electrophysiological marker of visual working memory," *PLoS One*, vol. 4, (no. 11), pp. e8042, 2009.

[89] P.J. Olesen, H. Westerberg, and T. Klingberg, "Increased prefrontal and parietal activity after training of working memory," *Nat Neurosci*, vol. 7, (no. 1), pp. 75-9, Jan 2004.

[90] G.D. Logan, "An instance theory of attention and memory," *Psychol Rev*, vol. 109, (no. 2), pp. 376-400, Apr 2002.

[91] M.R. Rueda, M.K. Rothbart, B.D. McCandliss, L. Saccomanno, and M.I. Posner, "Training, maturation, and genetic influences on the development of executive attention," *Proc Natl Acad Sci U S A*, vol. 102, (no. 41), pp. 14931-6, Oct 11 2005.

[92] J. Holmes, S.E. Gathercole, M. Place, D.L. Dunning, K.A. Hilton, and J.G. Elliott, "Working memory deficits can be overcome: Impacts of training and medication on working memory in children with ADHD," *Applied Cognitive Psychology*, vol. 24, (no. 6), pp. 827–836, Sep 2010.

[93] K. Zinke, M. Zeintl, A. Eschen, C. Herzog, and M. Kliegel, "Potentials and limits of plasticity induced by working memory training in old-old age," *Gerontology*, vol. 58, (no. 1), pp. 79-87, 2012.

[94] F. Zehnder, M. Martin, M. Altgassen, and L. Clare, "Memory training effects in old age as markers of plasticity: a meta-analysis," *Restor Neurol Neurosci*, vol. 27, (no. 5), pp. 507-20, 2009.

[95] L.L. Richmond, A.B. Morrison, J.M. Chein, and I.R. Olson, "Working memory training and transfer in older adults," *Psychol Aging*, vol. 26, (no. 4), pp. 813-22, Dec 2011.

[96] C. Zhang, C.C. Kuo, A.W. Chiu, and J. Feng, "Prediction of S-glutathionylated Proteins Progression in Alzheimer's Transgenic Mouse Model Using Principle Component Analysis," *J Alzheimers Dis*, vol. 30, (no. 4), pp. 919-34, Jan 1 2012.

[97] T.J. De Bock, S. Das, M. Mohsin, N.B. Munro, L.M. Hively, Y. Jiang, C.D. Smith, D.R. Wekstein, G.A. Jicha, A. Lawson, J. Lianekhammy, E. Walsh, S. Kiser, and C. Black, "Early Detection of Alzheimer's Disease Using Nonlinear Analysis of EEG via Tsallis Entropy," *Conf Proc Biol Soc Eng* vol. 2010, pp. 1-4, 2010.

[98] J.M. Palva, S. Monto, S. Kulashekhar, and S. Palva, "Neuronal synchrony reveals working memory networks and predicts individual memory capacity," *Proc Natl Acad Sci U S A*, vol. 107, (no. 16), pp. 7580-5, Apr 20 2010.

[99] A. Gazzaley, W. Clapp, J. Kelley, K. McEvoy, R.T. Knight, and M. D'Esposito, "Age-related top-down suppression deficit in the early stages of cortical visual memory processing," *Proc Natl Acad Sci U S A*, vol. 105, (no. 35), pp. 13122-6, Sep 2 2008.

[100] M.M. Moore, "Real-world applications for brain-computer interface technology," *IEEE Trans Neural Syst Rehabil Eng*, vol. 11, (no. 2), pp. 162-5, Jun 2003.

[101] L.D. Liao, C.Y. Chen, I.J. Wang, S.F. Chen, S.Y. Li, B.W. Chen, J.Y. Chang, and C.T. Lin, "Gaming control using a wearable and wireless EEG-based brain-computer interface device with novel dry foam-based sensors," *J Neuroeng Rehabil*, vol. 9, pp. 5, 2012.

[102] C.C. Kuo, W.S. Lin, C.A. Dressel, and A.W. Chiu, "Classification of intended motor movement using surface EEG ensemble empirical mode decomposition," *Conf Proc IEEE Eng Med Biol Soc*, vol. 2011, pp. 6281-4, 2011.

[103] T.P. Zanto, M.T. Rubens, A. Thangavel, and A. Gazzaley, "Causal role of the prefrontal cortex in top-down modulation of visual processing and working memory," *Nat Neurosci*, vol. 14, (no. 5), pp. 656-61, May 2011.

[104] W.C. Clapp, M.T. Rubens, J. Sabharwal, and A. Gazzaley, "Deficit in switching between functional brain networks underlies the impact of multitasking on working memory in older adults," *Proc Natl Acad Sci U S A*, vol. 108, (no. 17), pp. 7212-7, Apr 26 2011.

[105] N. Gates and M. Valenzuela, "Cognitive exercise and its role in cognitive function in older adults," *Curr Psychiatry Rep*, vol. 12, (no. 1), pp. 20-7, Feb 2010.

[106] C.C. Kuo, J.L. Knight, C.A. Dressel, and A.W. Chiu, "Non-invasive BCI for the decoding of intended arm reaching movement in prosthetic limb control," *Am J Biomed Eng*, vol. 2, (no. 4), pp. 155-162, Aug 2012.